PALEOCEANOGRAPHY, VOL. 8, NO. 6, PAGES 699-735, DECEMBER 1993

ON THE STRUCTURE AND ORIGIN OF MAJOR GLACIATION CYCLES
2. THE 100,000-YEAR CYCLE

J. Imbrie,[1] A. Berger,[2] E. A. Boyle,[3] S. C. Clemens,[1] A. Duffy,[1] W. R. Howard,[4] G. Kukla,[4] J. Kutzbach,[5] D. G. Martinson,[4] A. McIntyre,[4,6] A. C. Mix,[7] B. Molfino,[4] J. J. Morley,[4] L. C. Peterson,[8] N. G. Pisias,[7] W. L. Prell,[1] M. E. Raymo,[3] N. J. Shackleton,[9] and J. R. Toggweiler[10]

Abstract. Climate over the past million years has been dominated by glaciation cycles with periods near 23,000, 41,000, and 100,000 years. In a linear version of the Milankovitch theory, the two shorter cycles can be explained as responses to insolation cycles driven by precession and obliquity. But the 100,000-year radiation cycle (arising from eccentricity variation) is much too small in amplitude and too late in phase to produce the corresponding climate cycle by direct forcing. We present phase observations showing that the geographic progression of local responses over the 100,000-year cycle is similar to the progression in the other two cycles, implying that a similar set of internal climatic mechanisms operates in all three. But the phase sequence in the 100,000-year cycle requires a source of climatic inertia having a time constant (~15,000 years) much larger than the other cycles (~5,000 years). Our conceptual model identifies massive northern hemisphere ice sheets as this larger inertial source. When these ice sheets, forced by precession and obliquity, exceed a critical size, they cease responding as linear Milankovitch slaves and drive atmospheric and oceanic responses that mimic the externally forced responses. In our model, the coupled system acts as a nonlinear amplifier that is particularly sensitive to eccentricity-driven modulations in the 23,000-year sea level cycle. During an interval when sea level is forced upward from a major low stand by a Milankovitch response acting either alone or in combination with an internally driven, higher-frequency process, ice sheets grounded on continental shelves become unstable, mass wasting accelerates, and the resulting deglaciation sets the phase of one wave in the train of 100,000-year oscillations.

> Whether a glacier or ice sheet influences the climate depends very much on the scale....The interesting aspect is that an effect on the local climate can still make an ice mass grow larger and larger, thereby gradually increasing its radius of influence.
>
> Johannes Oerlemans [1991, p. 155]

1. BACKGROUND AND PURPOSE

Climate over the past half-million years has been dominated by glacial cycles with periods near 23, 41, and 100 kyr [Hays

[1] Department of Geological Sciences, Brown University, Providence, Rhode Island.
[2] Institut d'Astronomie et de Géophysique G. Lemaître, Université Catholique de Louvain, Louvain-la-Neuve, Belgium.
[3] Department of Earth, Atmospheric, and Planetary Sciences, Massachusetts Institute of Technology, Cambridge.
[4] Lamont-Doherty Earth Observatory, Columbia University, Palisades, New York.
[5] Center for Climatic Research and Space Science, University of Wisconsin, Madison.
[6] Department of Geology, Queens College, City University of New York, Flushing.
[7] College of Oceanography, Oregon State University, Corvallis.
[8] Rosenstiel School of Marine and Atmospheric Science, University of Miami, Miami, Florida.
[9] Godwin Laboratory for Quaternary Research, Cambridge, United Kingdom.
[10] Geophysical Fluid Dynamics Laboratory, NOAA, Princeton, New Jersey.

Paper number 93PA02751.
0883-8305/93PA-02751$10.00

et al., 1976]. Each cycle is linearly correlated with one of the parameters of the Earth's orbit that control the amount and distribution of incoming radiation: the precession index cycle, the obliquity cycle, and the 100-kyr cycle of eccentricity [Imbrie et al., 1984]. These statistical correlations support the Milankovitch theory, the central tenet of which is that astronomically driven variations in insolation cause significant changes in climate [Milankovitch, 1930]. In an earlier paper [Imbrie et al., 1992 (hereafter referred to as Part 1)] we examine the 23- and 41-kyr cycles in a geographic array of time series spanning the past 400 kyr (Table 1). From observations in this array, we conclude that each of these glaciation cycles can be explained as a linear response to variations in summer insolation at high northern latitudes, as in classic Milankovitch theory (section 6.1). The influence of insolation at other latitudes and seasons is discussed in section 3.2.2.

Our purpose in this paper is to describe and explain the 100-kyr glaciation cycle by examining an array of oceanic time series that monitor different components of the global system over the past 400,000 years. In one of these time series, the $\delta^{18}O$ record of global ice mass, the 100-kyr cycle has roughly twice the amplitude of the other two cycles combined. A search for a satisfactory explanation of this dominant feature of late Pleistocene history has been a major research theme since its discovery [Kukla, 1968; Mesolella et al., 1969; Broecker and van Donk, 1970; Shackleton and Opdyke, 1973; Hays et al., 1976]. At first glance, the strong correlation between eccentricity and $\delta^{18}O$ in the 100-kyr band suggests that the solution to the 100-kyr problem would fit neatly into Milankovitch theory. In fact, finding a satisfactory explanation has proved to be a major scientific challenge. One basic difficulty is that the amplitude of the 100-kyr radiation cycle seems much too small and its phase too late to drive the 100-kyr glaciation cycle (section 2).

Dozens of explanations have been suggested (section 4). Some models explain the cycle as a free, self-sustaining oscillation with no Milankovitch forcing [e.g., Saltzman and Maasch, 1988]. In models of this type, the 100-kyr cycle is

TABLE 1. Climatic Records Examined in This Paper

Code	Core	Data	Depth, m	Main Reference
2	5-core stack	Planktonic $\delta^{18}O$	3100	Imbrie et al. [1984]
3	3-site stack	Magnetic susceptibility measure of aridity	-1240	Kukla et al. [1990]
4	RC27-61	Dust flux from Arabia	1893	Clemens and Prell [1990]
5	K708-1	SST estimate from forams	4053	Ruddiman and McIntyre [1984]
7	RC11-120/E49-18	SST estimate from radiolaria		Hays et al. [1976]
[7]	RC11-120	SST estimate as above	3193	
[7]	E49-18	SST estimate as above	3254	
8	V19-30	$\Delta\delta^{13}C$ (surface minus deep)	3091	Shackleton and Pisias [1985]
9	5-core stack	$\Delta\delta^{13}C$ (surface minus deep)	3019	Curry and Crowley [1987]
12	P6408-9	CO_3 dissolution index	4098	Peterson and Cofer-Shabica [1987]
14	DSDP607	$\Delta\delta^{13}C$ index of ventilation	3427	Raymo et al. [1990]
[14]	DSDP607	$\delta^{13}C$ (benthic)	3427	
[14]	DSDP552	$\delta^{13}C$ (benthic)	2301	
[14]	ODP677	$\delta^{13}C$ (benthic)	3461	
15	AII107-131/-65	Cd/Ca phosphate proxy	2860	Boyle [1984*a*, *b*]
[15]	AII107-131	Cd/Ca phosphate proxy	2925	
[15]	AII107-65	Cd/Ca phosphate proxy	2795	
16	CH82-24-4PC	Cd/Ca phosphate proxy	3427	Boyle and Keigwin [1985]
17	V19-30	$\delta^{13}C$ (benthic)	3091	Shackleton and Pisias [1985]
18	V19-30	$\Delta\delta^{18}O$ index of deep temperature	3091	Shackleton [1987]
[18]	RC17-177	$\delta^{18}O$ (planktonic)	2600	Shackleton [1987]
19	K-11	Planktonic $\delta^{18}O$; percentage of G. bulloides; foram assemblage	2900	Kellogg et al. [1978]
20	RC13-229 and	$\Delta\delta^{13}C$ (deep AA values minus	4194	Oppo et al. [1990]
[20]	RC13-110	deep Pacific values)	3231	Mix et al. [1991]
21	EN120-GGC-1	Cd/Ca phosphate proxy	4450	Keigwin et al. [1991]
22	PS21295-4	Planktonic $\delta^{18}O$	3112	Jones and Keigwin [1988]
24	Troll 3.1	Planktonic forams	332	Lehman and Keigwin [1992*a*]
25	HM79-6/4	Diatom flux	900	Karpuz and Jansen [1992]
26	57-5	Diatom assemblage	1892	Karpuz and Schrader [1990]
27	V28-56	Planktonic forams/gram	2941	Kellogg et al. [1978]

Codes in brackets indicate an individual record combined with others to form a single climatic index. Table data is from Imbrie et al. [1992].

forced by internal climate system processes so that its phase is arbitrary with respect to eccentricity. Other models explain the cycle as a nonlinear interaction between orbitally forced responses (in the 23- and 41-kyr bands) and the internal dynamics of the atmosphere, oceans, ice sheets, and lithosphere [e.g., Maasch and Saltzman, 1990; Gallée et al., 1992]. In these, the phase of the 100-kyr cycle is orbitally influenced. Numerical models of this type, which are able to account for the statistical linkage that clearly exists between eccentricity and climate, provide the basis for our own conceptual model of the 100-kyr cycle (section 7).

The climatic processes that comprise our model are inferred from phase observations documenting the geographic progression of local responses over the 100-kyr cycle. As described in section 3 of Part 1, our focus is on the process of glaciation, especially on the role that the ocean at high latitudes and at depth plays in the complex of climatic mechanisms that lead to the growth and decay of great ice sheets. This focus has one unfortunate consequence, namely, that our array of time series is very sparse in low latitudes, where previous work has shown that changes in monsoon circulation and equatorial wind fields dominate local climate history [e.g., Prell and Kutzbach, 1987]. Our sampling strategy may well exclude evidence of low-latitude processes that could influence glaciation by changing the concentrations of water vapor and methane in the atmosphere.

2. THE 100-kyr CYCLE PROBLEM

Essential features of the 100-kyr cycle problem can be seen by partitioning climatic and radiation time series into their dominant periodic components (Figure 1). In both the 23-kyr (precession) and 41-kyr (obliquity) bands, the strong, linear correlations between radiation and $\delta^{18}O$ are now fairly obvious. The statistical significance of each correlation is easily confirmed by calculating the coherency, a correlation measure that allows for phase differences. In the 100-kyr band, however, the correlation is not obvious, owing to the small amplitude of the radiation oscillation. Yet from a statistical point of view, the linear relationship (coherency equals 0.91) is nearly as significant as that between $\delta^{18}O$ and insolation in the 23- and 41-kyr bands (0.95 and 0.90, respectively) (see Table 2). Moreover, the correlation in the 100-kyr band is a persistent feature of Earth history over the past several million years [Shackleton et al., 1990; Shackleton et al., 1993].

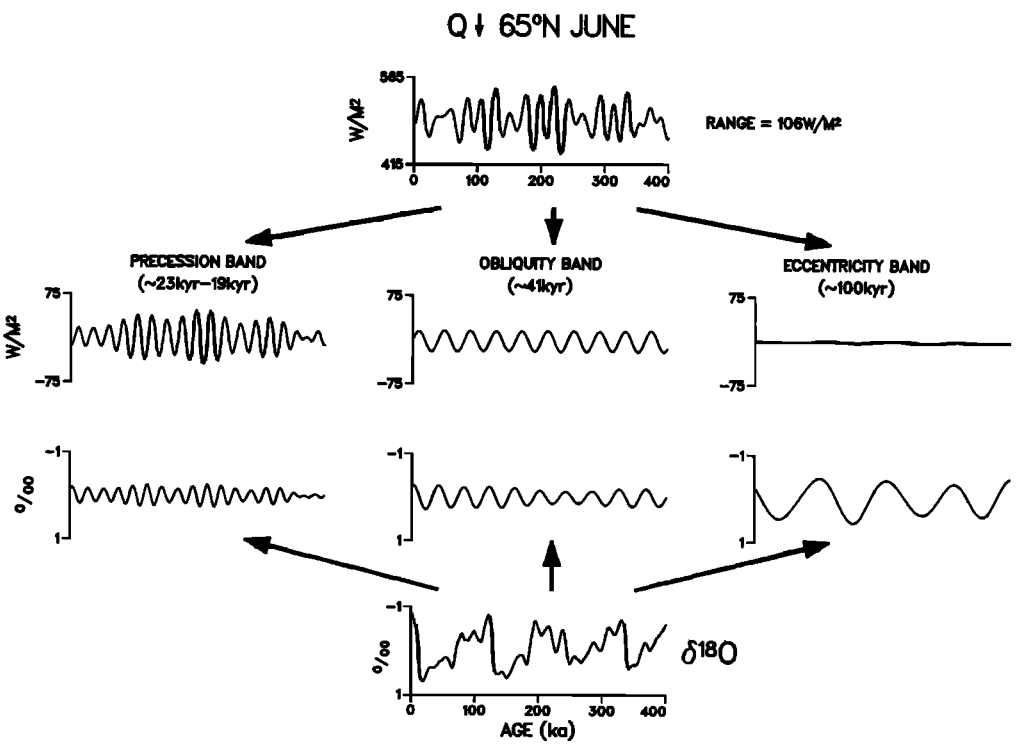

Fig. 1. The 100-kyr cycle problem as seen by partitioning radiation and climate time series into their dominant periodic components (in the precession, obliquity, and 100-kyr eccentricity bands). Radiation time series are from Berger [1978*a*]; $\delta^{18}O$ data are from Imbrie et al. [1984]. Partitioning is done using Hamming band-pass filters with a bandwidth of 0.019 kyr^{-1} for the 41- and 100-kyr bands and 0.036 kyr^{-1} for the 23-kyr band [Jenkins and Watts, 1968]. The $\delta^{18}O$ cycles at periods near 23, 41, and 100 kyr are so strongly correlated with astronomically driven radiation cycles as to suggest a causal linkage in all three bands. But these correlations for the 23-, 41-, and 100-kyr bands (coherencies of 0.95, 0.90, and 0.91, respectively, in Table 2) hide an intriguing physical problem. Why is the system's response so strong in the 100-kyr band? There the amplitude of the radiation signal (2 W m^{-2}) is 1 order of magnitude smaller than in the other two bands.

TABLE 2. Statistical Summary of Cross Spectra of Climatic Time Series

Number	Variable	100 kyr		41 kyr		23 kyr		k_o	T	Δt
		k	ø, deg	k	ø, deg	k	ø, deg			
1	Q↓ 65°N mid-June	—	—	0.91	- 78 ± 11	0.95	- 86 ± 9	0.66	400	2
2	Stack -$\delta^{18}O$	0.91	+13 ± 12	0.90	+80 ± 12	0.95	+87 ± 9	0.66	400	2
3	-China loess	0.89	+19 ± 13	0.79	+16 ± 20	0.69	+12 ± 26	0.66	400	1
4	-Arab. dust	0.96	+10 ± 8	0.80	+1 ± 19	0.94	+4 ± 9	0.66	400	2
5	K708-1 SST	0.99	+6 ± 2	0.98	+12 ± 6	0.91	+27 ± 15	0.82	260	2
6	V3097/607 SST	0.85	+3 ± 16	0.95	- 13 ± 9	0.94	+72 ± 9	0.66	400	2
7	SST 44°S	0.92	- 47 ± 11	0.93	- 14 ± 10	0.86	- 35 ± 15	0.66	400	2
8	$-\Delta\delta^{13}C$ (s-deep)	0.91	- 44 ± 13	0.89	- 32 ± 15	0.91	- 39 ± 12	0.71	343	1
9	$-\Delta\delta^{13}C$ (s-deep)	0.87	- 41 ± 18	0.88	- 57 ± 17	0.81	- 8 ± 22	0.79	280	1
10	$-\Delta\delta^{13}C$ (i-deep)	0.72	- 26 ± 25	0.76	+13 ± 23	(0.42)	+130 ± 46	0.69	366	3
12	CO_3 diss. Carib.	0.82	- 1 ± 18	0.92	+13 ± 11	0.76	- 1 ± 21	0.66	400	5
13	CO_3 pres. 45°S	0.91	- 12 ± 12	0.89	- 38 ± 13	0.91	+7 ± 12	0.66	400	2
14	$\Delta\delta^{13}C$ (%NADW)	0.87	+16 ± 15	0.86	+5 ± 16	0.83	+41 ± 17	0.66	400	3
15	-Cd/Ca 31°S	0.92	- 77 ± 13	0.78	- 49 ± 23	0.80	- 27 ± 22	0.76	302	5
17	$\delta^{13}C$ (deep)	0.92	- 14 ± 12	0.92	- 9 ± 12	0.95	+10 ± 10	0.71	343	1
20	$\Delta\delta^{13}C$ (deep-deep)	0.82	- 34 ± 18	0.84	- 36 ± 16	0.93	- 56 ± 10	0.66	400	3

Items tabled are coherency k, phase angle ø with 80% confidence interval, 80% test statistic for nonzero coherency k_o, age in kiloyears of oldest sample used in the calculation T, and uniform sampling interval Δt in kiloyears. Values for variable 2 are calculated versus orbital time series [Berger, 1978*a*] of eccentricity, obliquity, and the precession index ($-e \sin \omega$). Other variables are calculated versus variable 2 (SPECMAP stack $\delta^{18}O$). The signs of certain time series are changed to yield a definition of phase consistent with plotting conventions in Figure 4. Positive phases indicate that the named variable lags the reference variable. The parentheses indicate a value of k that is not significant at the 80% level. Bandwidth for all calculations is 0.01 kyr^{-1}. Statistical analysis has not been performed on time series shorter than 260 kyr. Data is from Imbrie et al. [1992].

Despite the strength and persistence of this correlation, attempts to use it as the basis for developing a theory of the 100-kyr cycle have experienced major difficulties. A review of these difficulties will provide a useful background for evaluating proposed models.

1. One difficulty in finding a simple Milankovitch explanation is that the amplitudes of all 100-kyr radiation signals are very small [Hays et al., 1976]. As an example, the amplitude of the 100-kyr radiation cycle at June 65°N (a signal often used as a forcing in Milankovitch theories) is only 2 W m^{-2} (Figure 1). This is 1 order of magnitude smaller than the same insolation signal in the 23- and 41-kyr bands, yet the system's response in these two bands combined has about half the amplitude observed at 100 kyr. Another 100-kyr insolation signal that has often been proposed as a forcing is the total radiation received by the planet over 1 year. Because the major axis of the Earth's orbit is a constant, increases in eccentricity cause an increase in this total. But the amplitude of this signal is also very small (less than 0.1% of the modern value). Thus, if the 100-kyr cycle is in fact forced externally by radiation changes having this periodicity, some form of resonance would be required to explain the heightened sensitivity in this frequency band (some mechanism broadly comparable, say, to the resonance responsible for the 4.1-day sea level cycle in the equatorial Pacific [Wunsch and Gill, 1976]). Hagelberg and Pisias [1991] have examined the statistical properties of Plio-Pleistocene time series in detail and have shown that these properties are, in fact, consistent with a linear resonance. The difficulty has been to find a physically plausible resonance mechanism that could amplify a low-amplitude free oscillation and achieve steady state in only three 100-kyr oscillations (section 7.1).

2. Another fundamental difficulty is that variations in eccentricity are not confined to periods near 100 kyr (Figure 2). In fact, during the late Pleistocene, eccentricity variations at periods near 100 kyr are of the same order of magnitude as those at 413 kyr (Figure 3). (In estimating the phase and amplitude of orbital variations over the past 400 kyr, we have used the calculations of Berger [1978*a*], which are slightly more accurate for this interval than those of Berger and Loutre [1991].) Yet the $\delta^{18}O$ record for this time interval has no corresponding spectral peak near 400 kyr. Like the "curious incident" of the dog that did not bark in the night, the absence of a response to a stimulus is an important clue. Thus any model of the 100-kyr cycle that depends on eccentricity must account for the lack of a response at periods near 400 kyr (the "400-kyr problem" of Imbrie and Imbrie [1980]). Again, one way around the problem is to postulate that the climate system exhibits some form of resonance at periods near 100 kyr.

3. As shown in Figure 2, the high coherency (0.91) observed between 100-kyr eccentricity and $\delta^{18}O$ signals is an average that hides significant amplitude mismatches, notably in Stage 11 about 400 ka (ka = 1000 years ago). Over this part of the record, as well as in Stage 1 (where digital filtering is not an accurate way of analyzing the problem), the $\delta^{18}O$ response is clearly not proportional to the postulated forcing. Moreover, if climatic responses other than $\delta^{18}O$ are examined, the disparity in amplitude of the responses in Stage 11 is even more apparent [e.g., Part 1, Figure 7, variables 6, 7, 12, 14, and 20]. Clearly, some differences in the amplitudes of individual waves in the train of 100-kyr cycles are caused by internal mechanisms that operate independently of any Milankovitch forcing.

4. These difficulties are compounded when we look back over the past two million years (Figure 3) and see that after its onset about one million years ago, the 100-kyr $\delta^{18}O$ cycle continues to increase in amplitude as the 100-kyr eccentricity cycle decreases.

5. Finally, if one assumes that the 100-kyr cycle is a linear response to a 100-kyr forcing, there is a significant dynamic problem in accounting for the small phase lag (13°) of the $\delta^{18}O$

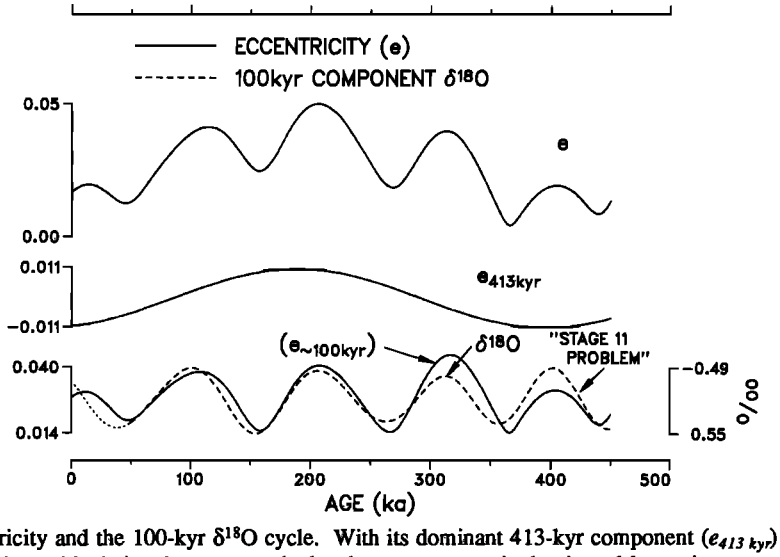

Fig. 2. Eccentricity and the 100-kyr $\delta^{18}O$ cycle. With its dominant 413-kyr component ($e_{413\ kyr}$) removed from eccentricity e, the residual signal $e_{-100\ kyr}$, calculated as $e - e_{413\ kyr}$, is dominated by variance over a moderately broad band of periods near 100 kyr [Berger, 1978*a*, *b*]. Averaged over the entire interval, this part of the eccentricity signal is coherent with the 100-kyr $\delta^{18}O$ cycle and leads it systematically by ~13°. But the $\delta^{18}O$ response is not proportional to eccentricity in Stage 11.

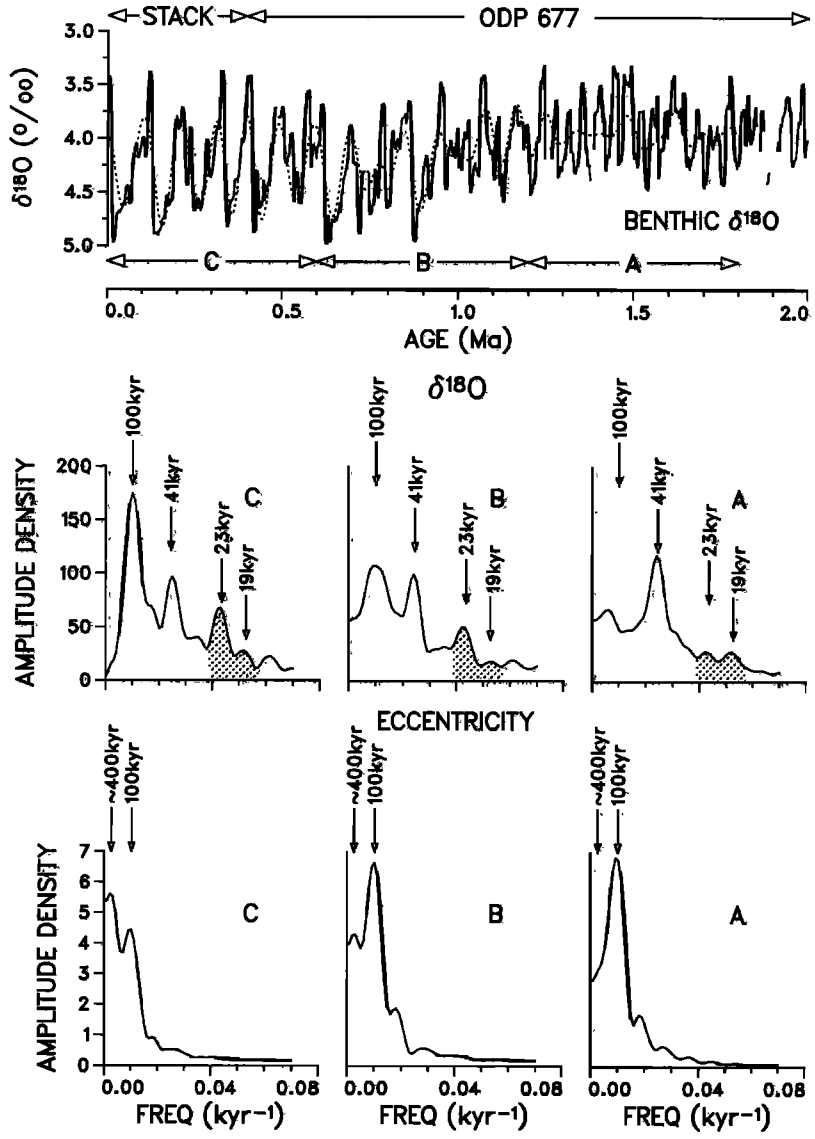

Fig. 3. Major orbital and glaciation cycles over the past two million years [Imbrie et al., 1993*a*]. (Top) A stacked benthic $\delta^{18}O$ record (based on data from Imbrie et al. [1992, Figure 5]) is combined with a benthic $\delta^{18}O$ record from Ocean Drilling Program (ODP) site 677 [Shackleton et al., 1990]. The dashed line is the 100-kyr cycle as defined by a band-pass filter. (Middle) The $\delta^{18}O$ spectra of intervals A, B, and C. Variability in the 19- to 23-kyr band is shaded to emphasize that increases here are nearly proportional to increases in the 100-kyr band. (Bottom) Eccentricity spectra of the same intervals, calculated from time series of Berger and Loutre [1991]. The 100-kyr eccentricity signal diminishes as the 100-kyr climatic cycle increases.

response (Table 2). Several lines of evidence (section 5) show that large ice sheets have a mean time constant of the order of 15 kyr. Without resonance or without an 8-kyr delay in the system's response, a linear, single-exponential system with a time constant of 15 kyr would be expected to lag any 100-kyr forcing by 43° (equation given in section 5.2). This is 30° more than the 13° response actually observed.

From the perspective of the Milankovitch theory, therefore, the essence of the 100-kyr problem is the difficulty of finding a physically plausible linear mechanism that would amplify the system's response to a small insolation forcing in a narrow band of periods near 100 kyr. In other words, the difficulty has been to propose a reasonable model whose response is governed by a differential equation with linear coefficients. As noted, one possibility is a linear resonance. But as reviewed in section 4, most theories of the 100-kyr cycle invoke either (1) a large-amplitude, self-sustaining, free oscillation that operates independently of any Milankovitch forcing, but which may interact with it to set the phase or (2) nonlinear interactions between orbitally forced responses and the dynamics of the

atmosphere, oceans, ice sheets, and lithosphere. These models are able to account for the statistical linkage that clearly exists between eccentricity and climate through the control that eccentricity e exerts on the amplitude of the 23-kyr precession index cycle, P ($P = e \sin \omega$, where ω is the longitude of perihelion measured from the moving vernal point [Berger, 1978*a*]).

3. STRATEGY AND METHODS

3.1. *Partitioning the Record*

The basic strategy we use in this paper is to partition each climatic record into its dominant frequency components in the 23-, 41-, and 100-kyr bands (Figure 1). This makes it possible to examine each of the three major cycles separately and to obtain evidence about the way in which the system responds to the forcing in each band. In studies of modern climate, the same statistical methods we use have been helpful in sorting out and evaluating the physical mechanisms that are responsible for cyclic phenomena at periods ranging from days to several years [Wunsch and Gill, 1976; Horel, 1982; Rasmusson and Carpenter, 1982]. On timescales ranging from thousands to millions of years, the approach has been used to show that quasi-periodic cycles in the Milankovitch and tectonic bands are superimposed on a simple background continuum that is presumed to originate stochastically [Shackleton and Imbrie, 1990].

Two circumstances make a partitioning strategy particularly appropriate for the Milankovitch problem. First, the nonlinear mechanisms driving the 100-kyr cycle must be very different from the linear mechanisms driving the 23- and 41-kyr cycles (section 2). Second, the geographic and seasonal pattern of insolation forcing in the precession band is very different from that in the obliquity band [Berger, 1979; Kukla and Gavin, 1992; Imbrie et al., 1993*a*]. For example, high obliquity results in greater insolation in the high latitudes of both hemispheres at the expense of low latitudes. These effects are strong in summer, negligible in autumn and spring, and in phase between the two polar hemispheres. These seasonal changes are accompanied by significant changes in the annual total insolation at all latitudes. In contrast, the precession of the equinoxes modifies seasonal insolation simultaneously over a broad band of latitudes that extends from one pole well into the opposite hemisphere. Moreover, the seasonal effects of precession are out of phase between the hemispheres, and the annual insolation totals are not affected.

Quite apart from these theoretical considerations, we have good stratigraphic evidence that the 41-kyr glaciation cycle has, in fact, evolved independently of the other two cycles over the past two million years (Figure 3).

Another line of evidence demonstrates the physical reality of climatic processes acting independently at each of the primary frequencies (1/23 kyr, 1/41 kyr, 1/100 kyr). In spectra of certain climatic variables, this evidence takes the form of discrete peaks that occur at frequencies representing nonlinear interactions between pairs of the primary climatic cycles. These peaks (interaction tones) suggest an origin similar to those which reflect nonlinear interactions between pairs of primary musical tones [Taylor, 1965] and pairs of primary tidal constituents [Munk and Cartwright, 1966]. In paleoclimatic spectra, observed interaction tones include 1/23 + 1/41 = 1/14.7, 1/41 + 1/100 = 1/29.1, and 1/23 - 1/100 = 1/29.9 [Pisias and Leinen, 1984; Pestiaux et al., 1988; Pisias and Rea, 1988; Ghil, 1989; Imbrie et al., 1989; Clemens and Prell, 1991]. Although the climatic processes responsible for such interactions have yet to be modeled satisfactorily, their existence does show that significant variation must originate as processes acting independently in the narrow frequency bands associated with major glaciation cycles.

3.2. *The Phase Sequence*

The remainder of this paper is an attempt to apply what we have observed and inferred in Part 1 about the mechanisms of the 23- and 41-kyr cycles, for which external forcings are clearly identified, toward a solution of a problem in which the identity of the forcing is one of the major unknowns. The approach is based on our finding that the geographic progression of 11 of the system's local responses in the 100-kyr cycle, relative to the phase of the global $\delta^{18}O$ response, is approximately the same as the progression in the 23- and 41-kyr cycles (Figure 4). From these observations, which are based on an admittedly very limited database, we draw an important inference that guides further analysis: all three cycles involve the same set of atmospheric, oceanic, and cryospheric processes. We draw a second important inference from the phase separation that occurs between the groups of early and late responses. From this two-step response pattern we infer that the early responses are paced by elements in the climate system with short time constants, while the late responses are paced by the longer time constant of the northern hemisphere ice sheets.

The observational basis for these inferences is the sequence of phases we have determined by cross-spectral analysis between $\delta^{18}O$ and each of the 14 other proxy records which are long enough to provide meaningful statistics. As discussed in section 4.4 of Part 1, it is important to know how much each of the climatic responses varies around its mean as the system's characteristics change over a climatic cycle. An estimate of this range, given in Table 2 as an 80% confidence interval, can be compared with observations made in section 8.1.

Although the phases given in Table 2 and the methods used to estimate these quantities are described in detail in Part 1, it may be helpful at this point to summarize what the features of this phase sequence are, to review the way in which we have chosen to record this sequence, and to summarize the methods used to obtain this information.

3.2.1. *Sequence of climate responses.* Of the 14 long climate records examined (Table 2) (Part 1, Figure 10), 11 display approximately the same phase sequence in all three cycles (Figure 4*d*). Each of the three remaining variables exhibits a response in one frequency band that is either incoherent with $\delta^{18}O$ or has a position in the phase sequence that is different from its position in the other bands. These are variables 6 (Atlantic sea surface temperature (SST) at 41°N), 10 ($\Delta\delta^{13}C$ ventilation index of Pacific intermediate water), and 13 ($CaCO_3$ preservation index at 45°S). As in Part 1, we set these responses aside for later investigation and focus on the 11 climatic variables that exhibit a similar phase sequence. The elimination of variable 6 from our array of sites is particu-

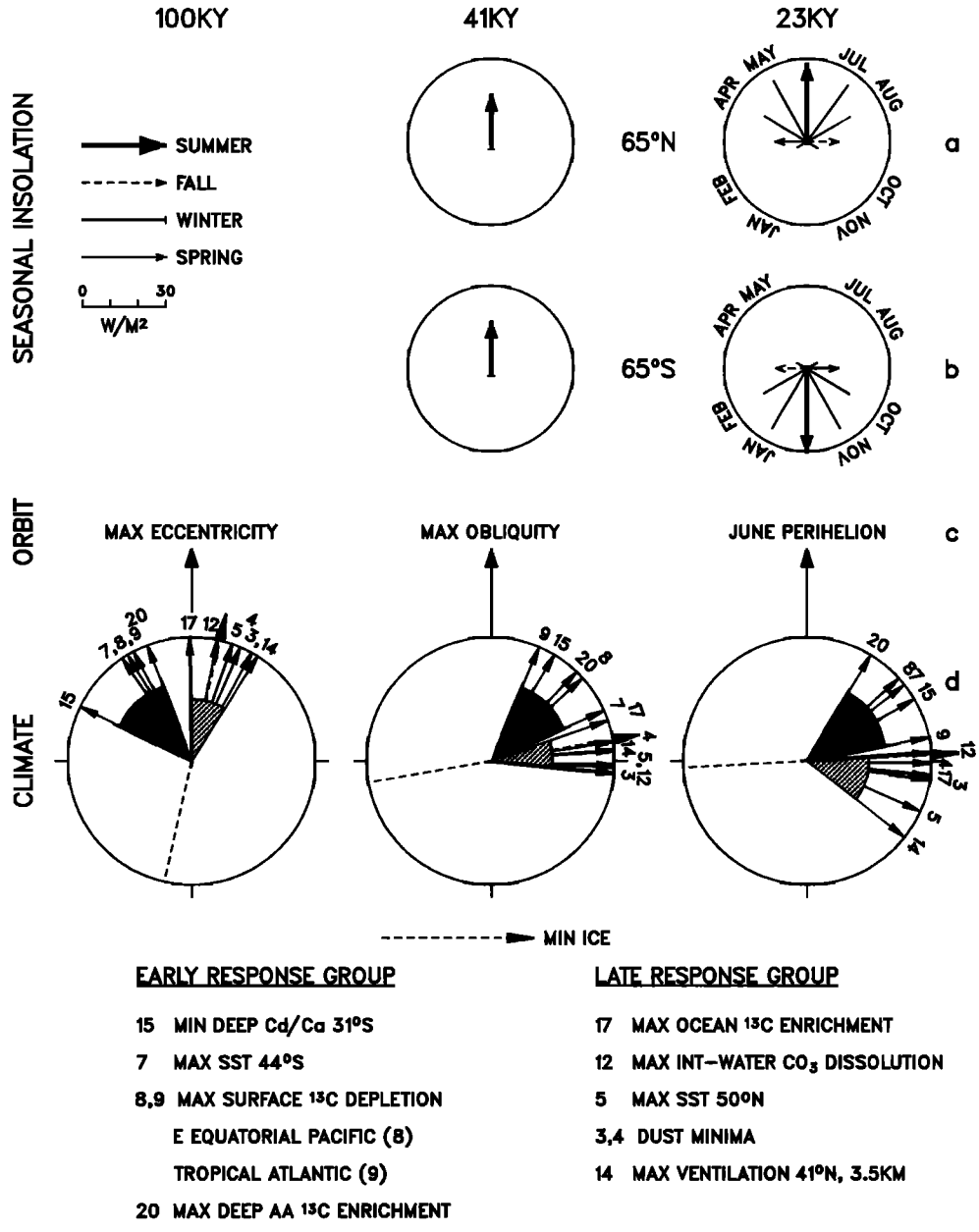

Fig. 4. Phases and amplitudes of Milankovitch insolation cycles at 65°N and 65°S compared with the phases of major glaciation cycles. (*a* and *b*) Angles of vectors with heads show the phases of maximum seasonal insolation at the solstices and equinoxes; vectors without heads show midmonth phases for other parts of the seasonal cycle; vector lengths show the amplitudes of insolation cycles of the past 400 kyr [Berger, 1978*a*, *b*]. (*c*) Orbital configurations defining zero phase in each band. (*d*) Phases of climatic variations in the three major glaciation cycles over the past 400 kyr (Table 2) (Part 1, Figure 10). See sections 3.1 and 3.2.2 for a discussion of insolation phases.

larly unfortunate, because it records a conspicuous but puzzling feature of the precession-driven climate cycle: a warming of one part of the surface Atlantic that lags the ice minimum by nearly a quarter of a cycle so as to be essentially out of phase with the high-latitude radiation signal [Ruddiman and McIntyre, 1984]. As noted in section 5.3 of Part 1, this "lagging warmth" pattern of the 23-kyr SST response can be mapped over a quadrant of the northeast Atlantic that extends from 54°N to 18°N and as far west as 21°W [Imbrie et al., 1989]. Although none of the hypotheses that have so far been advanced to explain this phenomenon strikes us as satisfactory, it seems probable that the transfer of moisture and heat to the atmosphere in this area plays an important role in the physics of the 23-kyr glaciation cycle.

3.2.2. *Plotting conventions and the Milankovitch link.* The three vector fans in Figure 4, each of which represents the sequence of local climatic responses as measured against the phases of $\delta^{18}O$, could be oriented in different ways. For example, we might choose to orient the fans with respect to the phase of insolation at some particular latitude and season. However, given the complexity of the full Milankovitch forcing field (Figures 4*a* and 4*b*), and the likelihood that the system responds to insolation at many different places and seasons (with sensitivities changing as the glacial cycle progresses), we choose instead to use a more objective set of reference vectors. These are the orbital configurations noted in Figure 4*c* (maximum eccentricity, maximum obliquity, and June perihelion).

With these definitions, zeros on the insolation phase wheels (Figures 4*a* and 4*b*) correspond to mid-June insolation for 65°N, which is a forcing we have good reason to believe is important in driving the glaciation cycles [Kukla et al., 1981]. In fact, from the evidence and physical arguments reviewed in section 6.3 of Part 1 we conclude that northern hemisphere summer radiation is an important, but by no means exclusive, element in the external forcing for the glaciation cycles. Insolation curves for other latitudes and seasons must also play significant roles in forcing the glaciation cycles. For example, insolation in the equatorial belt of the oceans could play an important role in the first part of the glacial cycle [Crowley et al., 1992; Kukla and Gavin, 1992]. And Genthon et al. [1987] argue for the importance of the total annual insolation at high southern latitudes. Because this high-latitude signal has spectral power only at 41 kyr and is exactly on phase with obliquity, it is unfortunately not possible to distinguish statistically between its influence and the influence of 41-kyr annual or seasonal cycles at any latitude poleward of 14° [Imbrie et al., 1993*a*]. Thus the mid-June 65°N time series shown in Figure 1 (like the early June 65°N time series used later in this paper as a forcing for our model) should properly be regarded only as a proxy for a combination of physically important seasonal and latitudinal elements in the full insolation forcing field.

3.2.3. *Methods.* The stratigraphic methods we have used to obtain the phase information in Figure 4 are fully discussed and referenced in Part 1. In essence, we use the oceanic $\delta^{18}O$ record in each core to construct a common temporal framework within which to measure the timing and phase of local climatic events with respect to the timing and phase of global $\delta^{18}O$ events. The precision with which this framework can be used is affected by a number of factors, including variations in the magnitude of the local component of the $\delta^{18}O$ signal (see sections 4.1 and 4.4 in Part 1).

To convert measurements made in the depth domain into estimates of absolute phase, we have chosen to transfer the Spectral Mapping Project (SPECMAP) chronology [Imbrie et al., 1984] to the $\delta^{18}O$ record observed in each core. If a different $\delta^{18}O$ chronology were chosen, the observed order of climatic events and phases would be unchanged. As an experiment, we have transferred the chronology developed for a groundwater $\delta^{18}O$ record in Nevada [Winograd et al., 1992] to the 11 cores in Figure 4. Although there is good evidence that the transfer of this quite different chronology to ocean cores is inappropriate [Imbrie et al., 1993*b*], this experiment confirms our expectation that essential features of the phase sequence would be unchanged. Thus the two-step response pattern that forms the basis of our analysis is a very robust feature of the data.

3.3. *Data.* The observations on which this study is based have already been published (see Table 1 in Part 1). Our contribution is to place these records in a common chronology and to analyze them statistically in exactly the same way. All time series described in this paper are available in digital form as SPECMAP Archives 2 and 4 at the National Center for Atmospheric Research and at the National Geophysical Data Center, both in Boulder, Colorado. For each oceanic record, the archives contain not only the original depth-in-core observations, but also the ^{14}C or $\delta^{18}O$ measurements we have used to convert the depth series into a time series.

4. REVIEW OF 100-kyr MODELS

Two theoretical studies by J. Weertman form the basis of many models that simulate the time-dependent behavior of Pleistocene ice sheets. The first study [Weertman, 1964] shows that large ice sheets have time constants of the order of 10-20 kyr. Because these calculated values are of the same order as the characteristic times of precession and obliquity cycles (11.5 kyr and 20.5 kyr), the response of the climate system cannot be linear with respect to the buildup and decay of large ice sheets, unless that response involves a linear resonance [Imbrie and Imbrie, 1980; Oerlemans, 1991]. The key role that ice sheet time constants play in glacial dynamics is illustrated by models that generate free oscillations at periods near 100 kyr. The "restoring force" that produces such oscillations is simply the delayed interaction between negative feedbacks (which have long time constants because they are linked to ice mass) and positive feedbacks which have short time constants [Saltzman, 1978].

The second study [Weertman, 1974] shows that Milankovitch insolation variations may indeed create large ice sheets through a feedback between ice accumulation rate and surface elevation. The importance of this feedback has been demonstrated in experiments with more detailed models [e.g., Le Treut and Ghil, 1983; Gallée et al., 1992]. Although many other feedbacks must influence the glaciation process, including those involving the albedo of periglacial areas, the temperature and chemistry of the ocean, the isostatic depression of the crust, subglacial meltwater, and the grounding-line dynamics of marine ice sheets, Oerlemans [1991] concludes that key processes initiating the growth and decay of ice sheets are linked not to the global energy budget but to the local climatological conditions at the surface of ice sheets.

Most models of the 100-kyr problem can be placed in one of seven groups (Table 3). Although some key assumptions are very different, these models are alike in that each invokes a set of internal feedbacks to convert some of the system's available potential energy, which originates externally and is assumed to be constant, into kinetic form and channel that energy into the 100-kyr band [Peixoto and Oort, 1984; Ghil and Childress, 1987].

4.1. *Models With Free Oscillations (Class I)*

In models of class I, sets of feedbacks are designed so that the system, when subjected to any broadband forcing, yields a

TABLE 3. A Short List of 100-kyr Cycle Models

Conceptual Model	Numerical Example
*Class I. Models With Free Oscillation**	
Group 1. Nonlinear resonance with a damped oscillation (P_i ~50 kyr)	Birchfield and Ghil [1993]
Group 2. Nonlinear resonance with a self-sustaining oscillation (P_i << 100 kyr)	Le Treut and Ghil [1983] Ghil [1991]
Group 3. Large, free oscillation (P_i ~100 kyr) with an arbitrary phase	Oerlemans [1982] Saltzman et al. [1982] Saltzman and Sutera [1987]
Group 4. Large, free oscillation (P_i ~100 kyr) with its phase set by orbitally forced responses at 23 kyr and 41 kyr	Oerlemans [1982] Saltzman et al. [1984] Maasch and Saltzman [1990]
Class II. Models Without Free Oscillation†	
Group 5. Simple rectification models (asymmetrical responses which extract power from the precession envelope)	Calder [1974] Imbrie and Imbrie [1980] Pisias and Shackleton [1984]
Group 6. Models which rectify the response to the orbital forcing by resolving regional components of the seasonal energy budget	Short et al. [1991] Crowley et al. [1992]
Group 7. Ice sheet models in which the isostatic response and ice mass balance are explicitly calculated	
Group 7a. Snow budget prescribed by a snow line related parametrically to insolation	Birchfield and Weertman [1978] Oerlemans [1980] Birchfield and Grumbine [1985] DeBlonde and Peltier [1991]
Group 7b. Snow budget calculated by an atmospheric model coupled to an ice sheet model	Pollard [1983] Gallée et al. [1991; 1992]

* Interactions between orbitally forced oscillations and free oscillations of the air-sea-ice-crust system with period P_i.

† Other nonlinear interactions between orbitally-forced responses and the dynamics of atmosphere, oceans, ice sheets, and asthenosphere.

free oscillation with period P_i that is either damped (group 1) or self-sustaining (groups 2-4). For one type of nonlinear resonance (group 1), P_i ~50 kyr. For another type (group 2) a self-sustaining oscillation with P_i << 100 kyr interacts with the external forcing in such a way that some of the energy of the internal oscillation is transferred to the 100-kyr band.

The distinctive feature of models in groups 3 and 4 is that the system's internal feedbacks maintain an oscillation at a period near 100 kyr in the absence of any band-limited external forcing. For example, in models proposed by Saltzman and his colleagues [e.g., Saltzman et al., 1982, 1984], feedbacks among three system elements (representing the ice sheets, ocean, and atmospheric CO_2) interact to produce a 100-kyr oscillation, even though the longest time constant (for the ice sheets) is set at a realistic value of 10 kyr. Although the model yields a 100-kyr cycle in the absence of any forcing (group 3), in the presence of orbital forcing the phase of this cycle is set by interactions between the internally driven cycle and the forced responses (group 4).

4.2. *Models Without Free Oscillations (Class II)*

When models of class II are forced away from equilibrium, negative feedbacks provide only a simple damping and return to equilibrium without oscillating. The 100-kyr cycle originates as a nonlinear response to orbital forcing and occurs only when this forcing is applied.

Models in group 5 explain the 100-kyr cycle by postulating a simple form of nonlinearity in which the system responds asymmetrically to forcings applied in "upward" and "downward" directions. Such a system extracts power from the

envelope of any amplitude-modulated forcing function. In the extreme case, where the response is zero to all forcings less than (or greater than) the mean, the output signal is said to be "rectified" or "clipped" [Short et al., 1991]. But any degree of asymmetry in the response will yield spectral peaks that are proportional to all the periods in the envelope (and their harmonics). Because the precession envelope in any Milankovitch forcing is precisely proportional to eccentricity (section 2) [Berger et al., 1992], all peaks in the eccentricity spectrum (and their harmonics) will appear in a rectified signal. This fact leads to a significant problem with all simple rectifier models of the late Pleistocene glaciation record. Although the output of these models contains significant 100-kyr power, their spectra are dominated by power extracted from the larger eccentricity peak near 400 kyr. As mentioned previously, such a dominance of 400-kyr power is not found in Pleistocene $\delta^{18}O$ records. For this reason, we rule out mechanisms in group 5 as the main cause of the 100-kyr glaciation cycle.

But we do not rule out the possibility that a rectification mechanism of the type described in group 6 might act in combination with processes described in our model (see section 7) to explain the 100-kyr glaciation cycle of the late Pleistocene [Pisias and Shackleton, 1984]. Models in group 6 are considerably more realistic than those discussed so far in that they resolve geographic components of the seasonal energy budget. Although they lack winds, ocean currents, and ice sheets, the simplicity of these models makes it possible to simulate time-dependent responses over long intervals. For example, using a linear version of the two-dimensional seasonal energy balance model, Short et al. [1991] show how regional patterns of yearly maximum temperatures vary over the past 800,000 years. These authors consider that this response in their model is a proxy for the seasonally integrated response of the monsoon system. In most geographic regions only 23- and 41-kyr peaks dominate the spectrum of this proxy, as would be expected from a linear model. But in equatorial areas, where the seasonal response results in temperature peaks at both equinoxes and the equinox nearest perihelion has the largest peak, the model's maximum-temperature response to the precessional forcing yields a rectified signal in which the amplitudes of 400- and 100-kyr peaks rival the amplitude of the peak in the 23-kyr band [Short et al., 1991; Crowley et al., 1992]. Because we find that the 100-kyr component of this signal is on phase with eccentricity, the possibility is worth considering that the climatic process represented in this model is part of the train of mechanisms that drives the 100-kyr glaciation cycle or determines its phase.

Models in group 7 explain the 100-kyr cycle by more complex forms of nonlinearity in the system's response to orbital forcing. The dynamics of selected parts of the climate system are simulated by feedback chains and allowed to interact with each other and (where appropriate) to respond to the Milankovitch forcing. To date, experiments with models of this type have concentrated on understanding three interacting elements in the dynamics of ice sheets: orbitally forced changes in the snow budget, the flow of ice, and the bedrock's response to ice loading. Each of the models in group 7a couples a different ice sheet—bedrock model to a simple snow budget model. Experiments aimed at simulating the ice-volume history of the late Pleistocene show that although this type of model can simulate the 100-kyr cycle, its ability to do so depends crucially on how the isostatic response is modeled. Unhappily, the use of a more realistic isostatic model does not lead to a better simulation [DeBlonde and Peltier, 1991].

Models which couple a less realistic ice sheet—bedrock model to a more realistic model of the snow budget (group 7b) can also simulate the 100-kyr cycle. Pollard's [1983] integration is long enough to show that the complex of feedbacks included in his model, which is simpler than the model of Gallée et al. [1992], is able to simulate the 100-kyr cycle without generating unwanted 400-kyr power. In one set of experiments, the latter model gives a reasonably satisfactory simulation of the past 120 kyr [Gallée et al., 1992]. Other experiments simulate the past 200 kyr [Gallée et al., 1993]. It remains to be seen if longer integrations will yield the 100-kyr ice volume cycle with a realistic Stage 11 and without producing an unrealistic 400-kyr cycle.

4.3. *Conclusions*

We draw two conclusions from this review. First, the essential condition for developing a 100-kyr cycle is the existence of northern hemisphere ice sheets large enough to exert a strong influence on global climate and sluggish enough to pace feedbacks that drive oscillations at periods longer than 41 kyr. In experiments reported by Oerlemans [1982], for example, free oscillations appear in model runs whenever ice thickness exceeds a critical value. Depending on how model parameters are set, free oscillation periods range between 70 and 130 kyr. The appearance of oscillations as ice sheet size increases is discussed more fully by Ghil [1984] and by Ghil and Childress [1987].

Our second conclusion is that the most likely explanation for the late Pleistocene 100-kyr glaciation cycle lies somewhere in the dynamic continuum between two model groups in Table 3: groups 3 and 7. Models of group 3 explain the 100-kyr cycle as a self-sustaining, internal oscillation paced by the large time constant of ice sheets. Here external forcing plays no role, and the phase of the oscillation is arbitrary with respect to orbital variations. However, Hagelberg and Pisias [1991] find that the higher-order statistical properties of models of this type are inconsistent with data.

Models of group 7, like those of group 1, explain the cycle as a nonlinear response to orbital forcing. Here the system acts as a nonlinear amplifier that channels energy into the 100-kyr band through feedbacks paced by the large time constant of ice sheets. In this case, the phase is set primarily by the attainment of thresholds in the system's response to the precessional forcing. Between the extremes of groups 3 and 7, in models of group 4, the 100-kyr cycle occurs as an internal, self-sustaining oscillation whose phase is set by the externally forced response to precession. Conceivably, the climate system has evolved in such a way that at different times in Earth history, a different balance of mechanisms is responsible for setting the phase of a particular 100-kyr oscillation (section 8.2.2).

5. MODELING THE PHASE SEQUENCE

As indicated in section 3, our approach to the 100-kyr problem is based on the progression of responses observed in phase spectra of the three major glaciation cycles. The qualitative

similarity of the three phase sequences provides a basis for developing a conceptual model of the governing processes (see section 7 and Part 1, section 6.5). Our aim in this section is to build a highly parameterized "system model" that will provide a quantitative explanation for the observed phase sequence in all three cycles. As a first step in this modeling enterprise we take advantage of the phase clusters documented in our data. Specifically, we simplify the modeling problem by postulating n discrete sources of inertia in n discrete climatic subsystems (n being the smallest number consistent with our data). Eventually, it may be possible to predict the observed phases with a set of coupled differential equations. Such a model would be capable of predicting a continuum of responses in phase spectra.

In the remainder of this section we will reexamine the evidence for phase clustering (section 5.1), extend the model developed in Part 1 so that it includes the 100-kyr cycle (sections 5.2 and 5.3), and then consider the implications of the resulting system model (section 5.4).

5.1. *The Phase Pattern*

When observations of mean phases obtained from cross spectra are displayed on phase wheels (Figure 4*d*), they fall in two clusters, one representing a group of responses that lead $\delta^{18}O$ significantly (the "early response group") and the other representing responses that are on phase with or lag slightly $\delta^{18}O$ (the "late response group"). Because each measurement has a statistical uncertainty (Table 2), it is desirable, before extending our quantitative model, to examine the mean phases and their confidence intervals (Figure 5). This display shows that the observations in our limited data set are, in fact, consistent with the two-cluster hypothesis. But it is now also clear that four of the responses in the late group actually lag $\delta^{18}O$ in all three cycles. These laggards are variables 3 (Chinese dust), 4 (the flux of dust from Arabia), 5 (Atlantic SST at 50°N), and 14 ($\Delta\delta^{13}C$ index of deep Atlantic ventilation at 41°N). Significantly, each variable reflects a property of the land, the sea surface, or the deep ocean (Table 1) that can be reasonably interpreted as a response to wind field and water budget changes driven by the growth and decay of northern hemisphere ice sheets [Manabe and Broccoli, 1985]. For modeling purposes therefore, we designate the average phase of this subset of late responses as R_4, the $\delta^{18}O$ response as R_3, and the average of early responses as R_2. The symbol R_1 is reserved for the (as yet unobserved) initial response.

5.2. *Modeling the Phase of $\delta^{18}O$ in the 23- and 41-kyr Cycles*

Consistent with our conclusions in Part 1, we start the modeling by assuming that the 23- and 41-kyr cycles are responses of a linear, single-exponential system with one input (radiation) and one output ($\delta^{18}O$). For these cycles, we have, in fact, good evidence from the coherency spectrum that the $\delta^{18}O$ ice volume proxy is linear in the radiative forcing (coherencies of 0.95 and 0.90). If such a system is forced at frequency f, the phase lag ϕ depends on the nature of the system's response. We will assume that the system has a single-exponential response that can be characterized by a delay d and a mean time constant T. Then $\phi = 2\pi f d + \arctan 2\pi f T$ [Jenkins and Watts, 1968]. If $d = 0$, the phases observed at 23 and 41 kyr yield independent estimates of T (70 kyr and 37 kyr for the two bands, respectively) which are not only much larger than values estimated by ice sheet models [Weertman, 1964; Oerlemans, 1991] but are also inconsistent between the two cycles. However, if we solve simultaneously for d and T at both frequencies, the best fit solution we obtain by iteration (d = 1 kyr and T = 17 kyr) gives phase lags (93° and 78°) that match rather well the lags observed in both cycles (87° and 80°). This estimate of the time constant (17 kyr) lies well within the theoretical range and matches an empirical estimate made by a different method [Imbrie and Imbrie, 1980].

In the next section, where we expand this first-order dynamic model to include phase information about the 11 local responses, we will retain the idea (discussed in Part 1) that the initial (but as yet unobserved) response to forcing has a delay of 1 kyr. But to explain the entire phase sequence, it will then be necessary to replace the single 17-kyr time constant of our first-order model with a set of time constants that reflect the combined inertia of all modeled subsystems.

5.3. *Modeling the Phase of $\delta^{18}O$ and 11 Local Responses*

The system as a whole can now be modeled as a chain of four subsystems, S_i, each having a quantity of climatic inertia parameterized either as a delay d or time constant T. In developing this model, the structure of which is described in Figure 6, we take advantage of our finding that all three cycles are characterized by the same geographic progression of responses. From this we infer that the same subsystems control the responses in all three cycles. But we allow for the possibility that the quantity of climatic inertia in a particular subsystem may differ from one cycle to another. To account for an initial response R_1, as well as responses R_2, R_3, and R_4, we require four subsystems acting in series. As speculations to guide research, model subsystems with particular elements in the real global system are identified in Figure 6.

When S_1 is subject to forcing, the response R_1 becomes the forcing for other subsystems further down the causal chain. Thus the phases of variables designated R_2 - R_4 reflect the time constants of a chain of subsystems (S_2 - S_4) driven by the initial response R_1. The numerical problem of accounting for the phase observations is now reduced to finding three time constants which, added to the delay, yield a cumulative pattern of responses that matches observations. Because responses are calculated at three frequencies simultaneously, this inverse problem is rather tightly constrained. For subsystems S_2, S_3, and S_4 our iterative, best fit numerical solution to this problem gives values of 3, 5, and 0.5 kyr, respectively, for the 23- and 41-kyr bands. Significantly, in the 100-kyr band this solution gives the same values for subsystems S_2 and S_4, but a much larger value for S_3 (15 kyr).

We interpret the 1-kyr delay as reflection of the largest source of inertia in the interacting cluster of initial-response mechanisms within subsystem S_1 (and suggest that these mechanisms include variations in northern hemisphere snow fields, sea ice, winds, boreal vegetation, and ice sheet margins). Expressed as a phase angle, the delay in the R_1 response is 16° at 23 kyr, 9° at 41 kyr, and 4° at 100 kyr

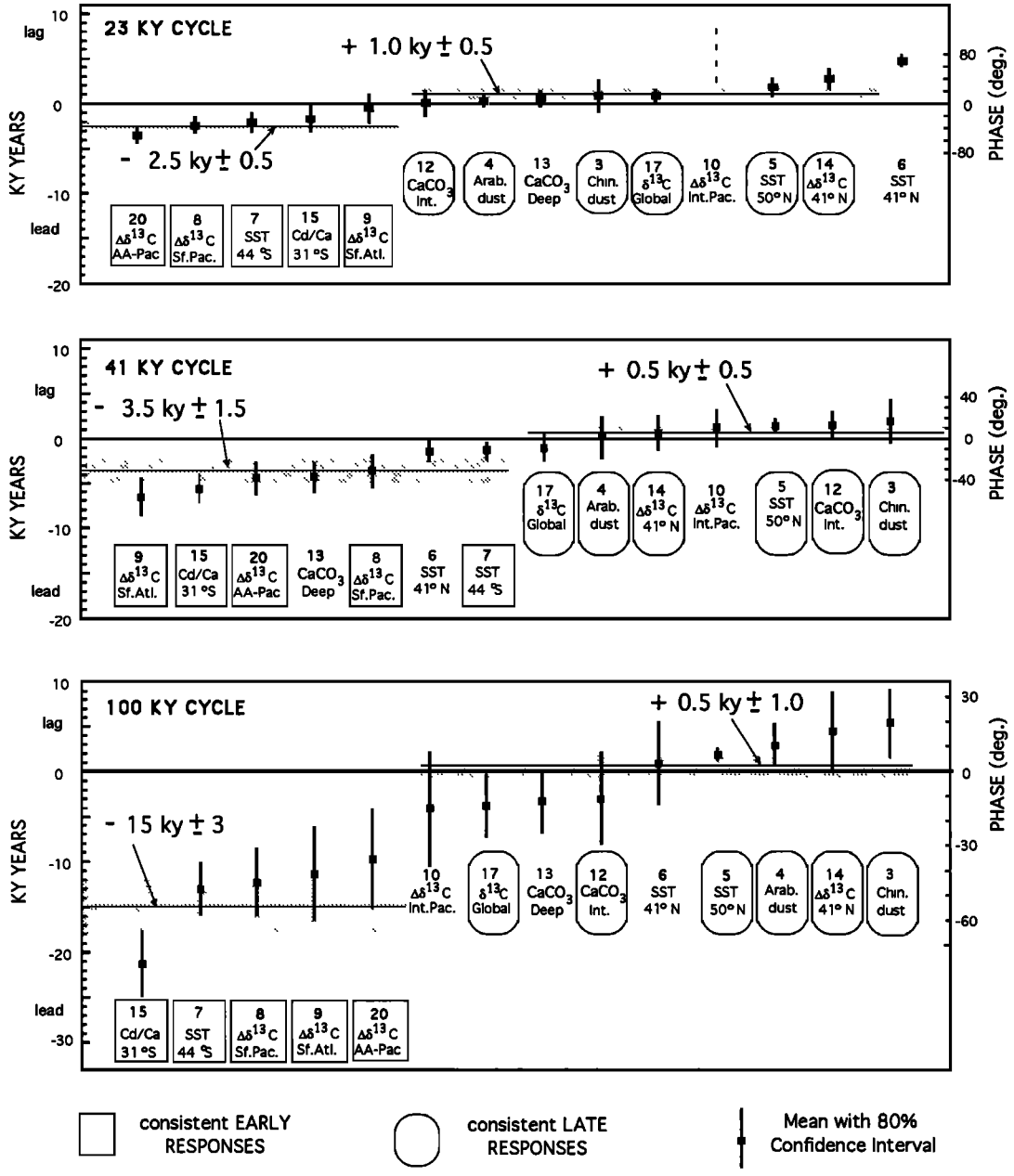

Fig. 5. Mean time and phase lags of 14 system responses measured with respect to $\delta^{18}O$ at the main periods of oscillation (Table 2). Responses of 11 variables are consistent over the three frequency bands. Statistically, these 11 responses fall into two groups. On Figures 6 and 7, the early responses are designated R_2 and the $\delta^{18}O$ response is designated R_3. Four late responses, designated R_4, lag $\delta^{18}O$ in all three cycles. Locations are given in Figure 11 and documentation in Table 1 and in Part 1 (Table 1).

(Table 4). In the 23- and 41-kyr bands, these phase angles can be used to begin the construction of phase portraits, that is, the model phase wheels in Figure 7 that display the subsystem responses to the forcing in each band. The 23- and 41-kyr portraits are easily completed, because the phase angles with respect to the radiative forcing Q can be obtained from the measurements in Table 2 (Q versus R_3, R_3 versus R_2 , and R_3 versus R_4). In the 100-kyr band, however, matters are not so simple, because we have purposely avoided identifying the forcing function or making assumptions about its phase. Here eccentricity is only a convenient and somewhat arbitrary reference signal against which to measure the phase of responses

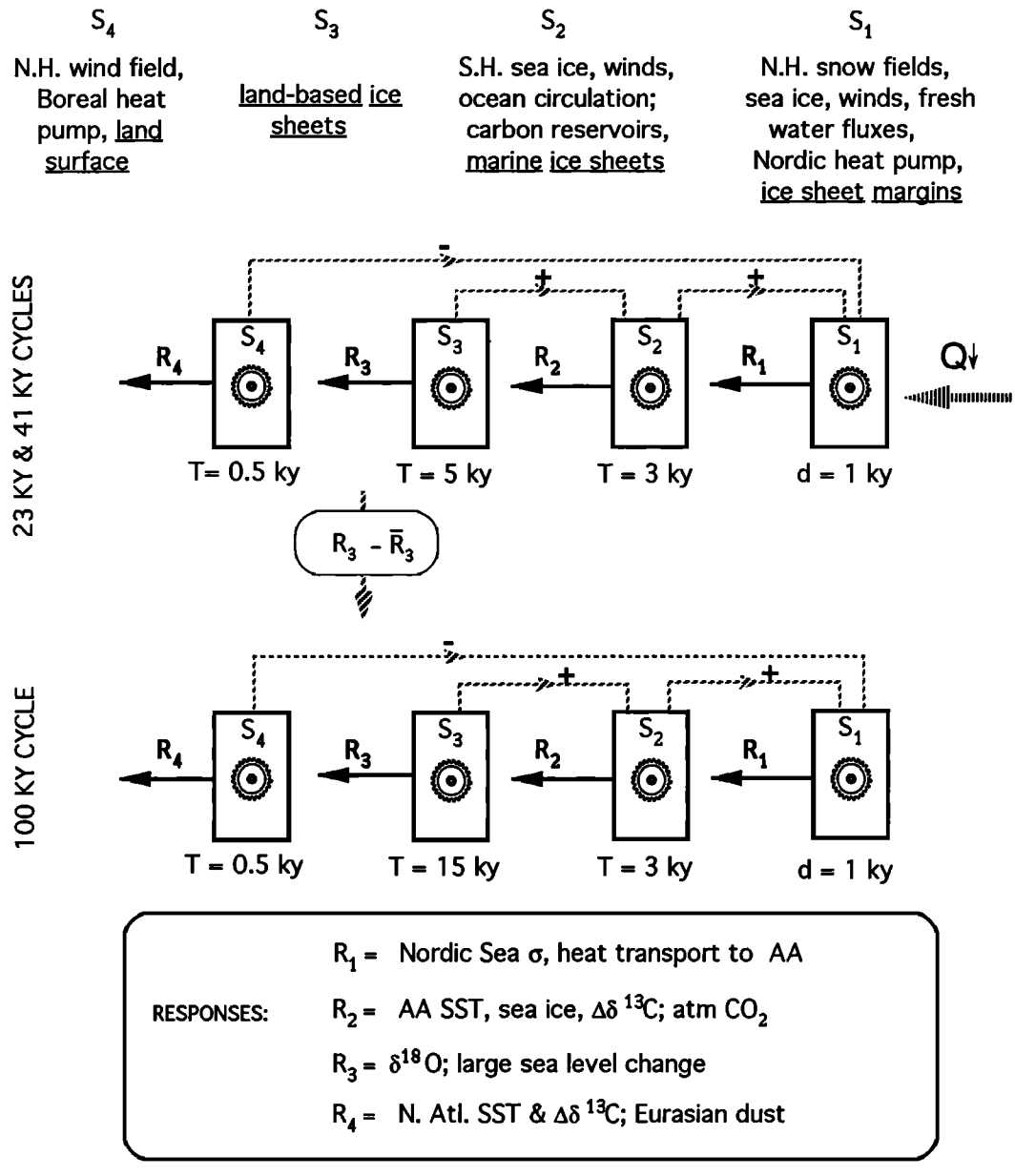

Fig. 6. System model of major glaciation cycles. To explain the observed phases in the response sequence R_i, sources of inertia (underlined) are postulated that control the rate at which changes are propagated through a chain of linear subsystems S_i, each having either a delay d or a time constant T. In the 23- and 41-kyr cycles, the initial response is driven by incoming radiation Q. In the 100-kyr cycle, the driving is a set of feedbacks operating whenever ice mass and sea level (R_3) depart significantly from the mean. These feedbacks combine to generate an internal thermal forcing (ITF in Figure 7). The same subsystems account for the observed responses in all three cycles, but a larger time constant is assigned to S_3 to account for the observed phase of R_3 in the 100-kyr cycle.

R_2 - R_4. To find the phase of the initial, unknown forcing we calculate the cumulative phase angle R_1 - R_3 (Table 4). The result of this calculation (58°) fixes the phase of the forcing function required by our linear model of the 100-kyr glaciation cycle. It is this forcing that we now identify with the theoretical concept of internal thermal forcing (ITF) developed in section 5.4.1.

As shown in Figure 7, the predicted phase sequence fits within the confidence intervals of the observations in all three cycles—provided we make a small change in one of our basic assumptions about insolation forcing due to precession. This assumption, described in section 3.2.2 and shown in Figure 4, is that the global insolation field that occurs when the moving perihelion point coincides with the northern hemisphere (June)

TABLE 4. Gain and Phase of the SPECMAP Systems Model

Model Element	Inertial Parameter, kyr	Normalized gain G at frequency f			Cumulative phase $\Sigma\phi_i$ at frequency f, deg		
		1/23 kyr	1/41 kyr	1/100 kyr	1/23 kyr	1/41 kyr	1/100 kyr
forcing	–	–	–	–	0	0	0
S_1	d = 1	1	1	1	16	9	4
S_2	T = 3	0.773	0.909	0.983	55	33	14
S_3	T = 5	0.591	0.794	–	109	71	–
S_3	T = 15	–	–	0.728	–	–	58
S_4	T = 0.5	0.991	0.997	1.000	117	75	59
Cumulative Gain, G (S_1-S_3)		0.457	0.722	0.715	–	–	–

The inertia of each subsystem is parameterized as a simple delay d or time constant T. Columns 3-5 give the normalized, steady state gain G of single-exponential subsystems S_i in response to unit changes in the forcing at different frequencies, where $G = [1 + (2\pi fT)^2]^{-1/2}$. Bottom row shows the cumulative normalized gain of the ice mass response S_3, given by the triple product ΠG_i (i = 1-3). The phase lag $\phi_i = 2\pi fd$ + arc tan $2\pi fT$, and the cumulative phase = $\Sigma\phi_i$ [Jenkins and Watts, 1968].

solstice is the maximum radiative forcing toward a full interglacial response (section 3.2.2). The insolation curve referred to as the "mid-June" insolation at 65°N is a time series representing one important geographic element in this forcing field (Figure 1). It is the assumption about mid-June perihelion that determines the zero point of the 23-kyr phase wheel in Figure 4. If, for example, we had assumed that the maximum interglacial forcing were the insolation field that occurs when perihelion coincides with the northern hemisphere (March) equinox, 90° would be added to all our phase measurements (Figure 4*a*). However, the phase of insolation time series in the 41-kyr obliquity band would be unaffected.

To produce the best fit between the 23-kyr phase measurements and our systems model, we have only to rotate the fan of model vectors counterclockwise about 20°. This corresponds to an assumption that the maximum forcing toward an interglacial is the radiation field striking the Earth when perihelion occurs in late May or early June. More precisely, we take the maximum precessional forcing as the insolation field occurring when the perihelion point has an angular distance of 21° from the summer solstice. This position is attained now on June 1, but during the past 600 kyr covered by our study, its calendar equivalent would have fallen at varying dates in late May or early June. Conveniently, the algorithm widely used for calculating radiation time series [Berger, 1978*b*] can be set for any desired season.

As discussed in section 3.2.2, the fact that we use the early June radiation curve for 65°N as the forcing for our highly parameterized model should not be taken to indicate that this element in the planetary radiation field is the only one of importance. We regard this curve simply as the most convenient single proxy for the combination of forcings which operate at many latitudes and seasons and actually cause global climate to change.

5.4. *Implications of the System Model*

5.4.1. *Internal thermal forcing.* Whatever the actual physical mechanisms of the 100-kyr cycle are, and whatever its primary cause, variations of thermal energy within the system are required to drive and modulate the processes that grow and melt ice sheets. In Figure 7 we designate this internal forcing as the "internal thermal forcing" (ITF) and calculate its position in the phase sequence as the cumulative phase produced by the inertia of the chain of subsystems that drives the ice sheets in our model (S_1 - S_3). As shown in Table 4, this model estimates that the phase of ITF with respect to ice volume is 58°. This inference is inconsistent with the idea that the 100-kyr cycle of glaciation is caused by an eccentricity-driven 100-kyr insolation cycle. Why? Because the 100-kyr radiation cycle leads $\delta^{18}O$ (R_3) by only 13°, whereas ITF leads $\delta^{18}O$ by 58°. Thus the phase of eccentricity is too late by about one-eighth of a cycle (58° - 13° = 45°), or by ~12 kyr, to be considered the main driver.

As shown in Figure 7, the postulated internal thermal forcing occurs within the quadrant of the 100-kyr sea level cycle that starts when the rate of sea level rise (dR_3/dt) reaches its maximum and ends when sea level (R_3) reaches its maximum. We note that this internal forcing need not and probably does not represent a single process but rather the sum of several 100-kyr processes, each with a particular amplitude and a particular phase (e.g., a methane process, a CO_2 process, an albedo process, a water vapor process, and a thermohaline process). In section 6.3 we review $\delta^{18}O$ evidence from the deep Pacific that supports the idea of a thermohaline process that changes deepwater temperatures at the predicted phase.

5.4.2. *Critical ice sheet size.* Oscillations of ice sheets in the 100-kyr cycle involve a larger quantity of climatic inertia (T = 15 kyr) and so have a more sluggish pace than oscilla-

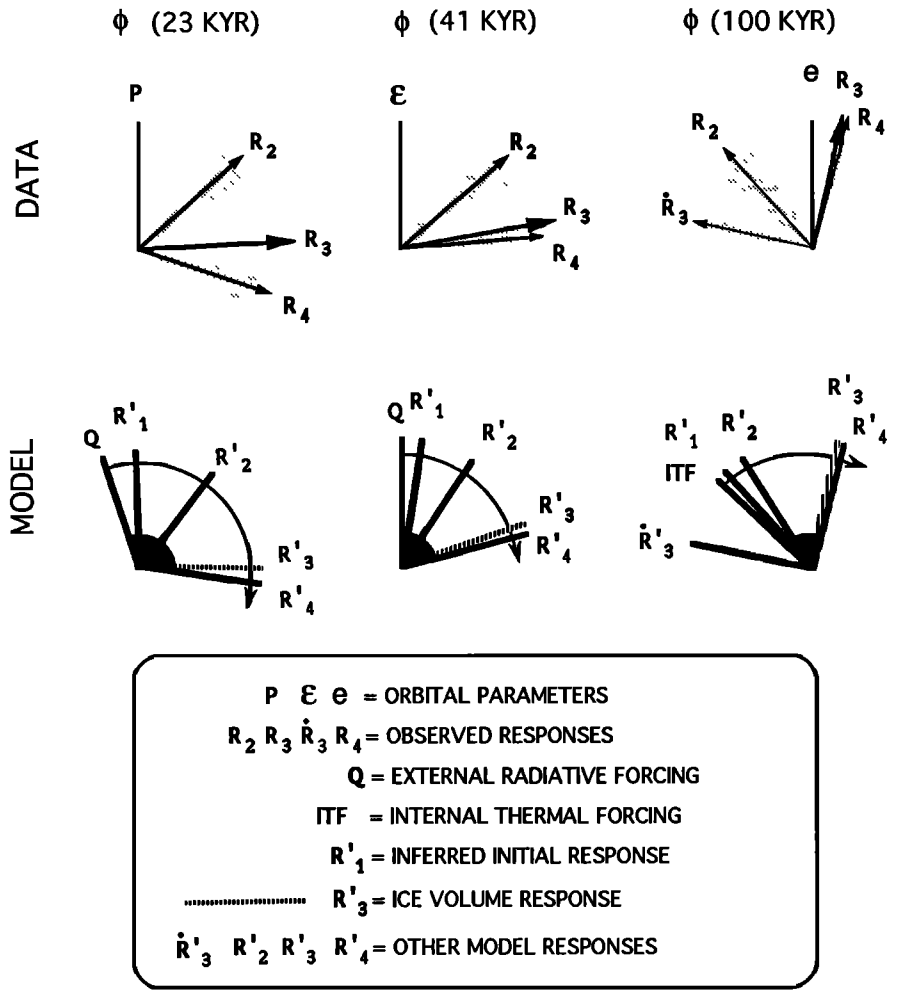

Fig. 7. Observed phase sequences compared with sequences calculated by the model described in Table 4 and Figure 6. Within uncertainties indicated by shading, each model sequence (R'_2, R'_3, and R'_4) matches the observed sequence of mean responses (R_2, R_3, and R_4) in all three cycles (Figure 5). R_3 is the ice mass response; its first derivative in the 100-kyr band is shown by the heavy dotted symbol. Q is the radiative forcing proxy, taken as insolation for early June at 65°N. The vector ITF shows the calculated phase of the internal thermal forcing. An arrowed arc shows the model's forcing and response in each cycle.

tions in the 23- and 41-kyr cycles (where $T = 5$ kyr). We take this to indicate that beyond some critical size, the behavior of ice sheets changes dramatically, as suggested by the modeling review in section 4.3. Our conceptual model uses this inference to help explain many features of the 100-kyr cycle, including its onset, pacing, and amplitude (section 7).

5.4.3. *Maximum ice sheet size.* According to the inertial parameters of our model, the maximum size an ice sheet will actually achieve in response to 100-kyr forcing is only 72% of the size it would achieve if allowed to reach equilibrium (Table 4). This might explain the discrepancies noted by W. R. Peltier (personal communication, 1992) between equilibrium estimates of ice distribution at the last glacial maximum and geophysical reconstructions based on sea level history.

5.4.4. *Ice sheets as climatic drivers.* Our system model, which is based on the phase observations shown in Figures 5 and 7, emphasizes the active role that ice sheets play in driving responses farther down the causal chain (R_4) by steering the winds and altering their properties [Manabe and Broccoli, 1985; Kutzbach and Guetter, 1986; Lautenschlager and Herterich, 1990]. A similar point is made by Oerlemans [1991].

6. LINEAR AND NONLINEAR COMPONENTS OF LONG TIME SERIES

6.1. *Linearity of Responses to Precession and Obliquity*

In studying physical systems that operate on an input to yield an output, the steady state response to a unit change in the input is defined as the gain [Jenkins and Watts, 1968, p. 12]. In many engineering applications it is usually easier and more meaningful to measure the gain of an operating system

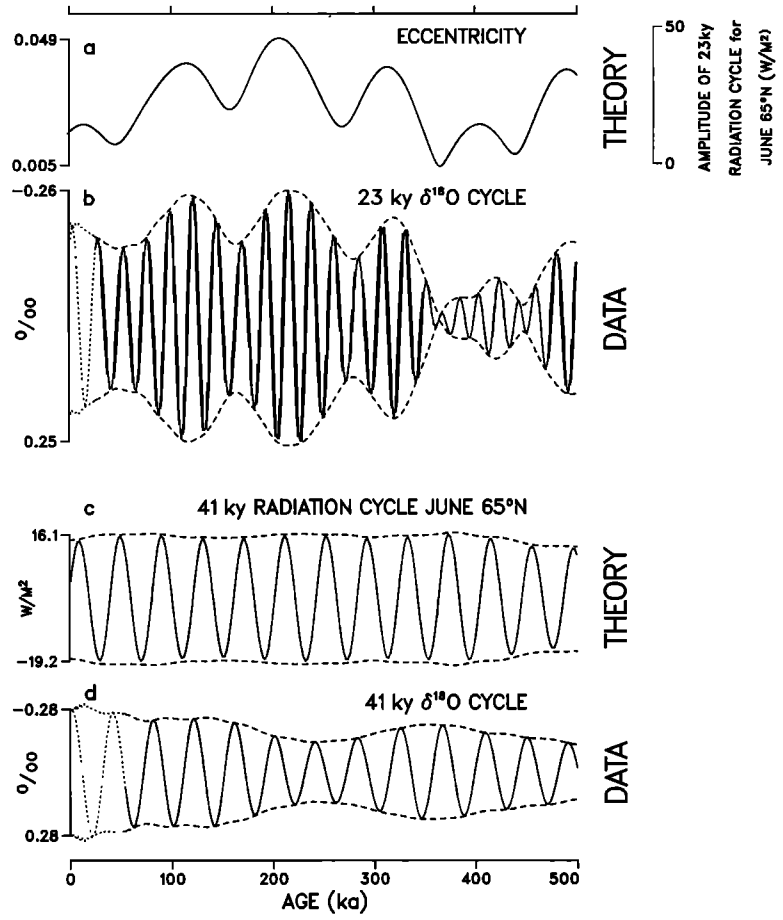

Fig. 8. Variations in the amplitude of $\delta^{18}O$ and radiation cycles. These modulations are linearly correlated in both the 23- and 41-kyr bands. (*a*) Eccentricity *e* as a function of time. The right-hand scale shows how eccentricity modulates the amplitude of the 23-kyr radiation cycle. (*b*) An enlarged view of the 23-kyr $\delta^{18}O$ cycle in Figure 1. The strong, nearly linear relationship between the amplitude of this cycle (dashed lines) and eccentricity shows that the glaciation process is essentially linear in this band. (*c* and *d*) Enlarged views of the 41-kyr radiation and $\delta^{18}O$ cycles in Figure 1. The approximately linear relationship between the envelopes of these cycles (dashed lines) shows that the process of glaciation is also essentially linear in this band. Orbital time series are from Berger [1978*a*, *b*] and $\delta^{18}O$ data are from Imbrie et al. [1984]. The 23-kyr and 41-kyr signals are obtained from Hamming filters with bandwidths of 0.036 kyr^{-1} and 0.019 kyr^{-1}, respectively. [Jenkins and Watts, 1968]. Dotted lines show where the exact form of the filtered curve is uncertain. Envelopes are obtained from Hilbert transforms of the filtered time series [Meskó, 1984].

by cross-spectral analysis of input and output data rather than by conducting experimental runs with a step change in the input. In this case, the steady state gain at a given frequency can be calculated as the ratio a_R/a_F, where a_R is the amplitude of the oscillating response and a_F is the amplitude of the forcing. Since the gain in linear systems is exactly proportional to the forcing, we can use astrogeological data (insolation and $\delta^{18}O$) on the operating climate system to measure its gain and see how linearly the system has behaved at the frequencies of precession and obliquity over the past 400 kyr. In fact, when time series of $\delta^{18}O$ and June insolation at 65°N are appropriately filtered, the amplitudes of the input and output signals are remarkably close to an exact proportionality (Figure 8). This is equivalent to saying that the system's gain during the late Pleistocene has been remarkably constant in the precession and obliquity bands or that the system has been linear and stationary (Figure 9). When examined in detail, however, the long-term trend in these curves suggests that the system has slowly evolved since ~250 ka so as to become more sensitive to the obliquity forcing.

6.2. *Components of the $\delta^{18}O$ Record*

The evidence for linearity just presented suggests a way of examining the 100-kyr cycle without the "distractions" pro-

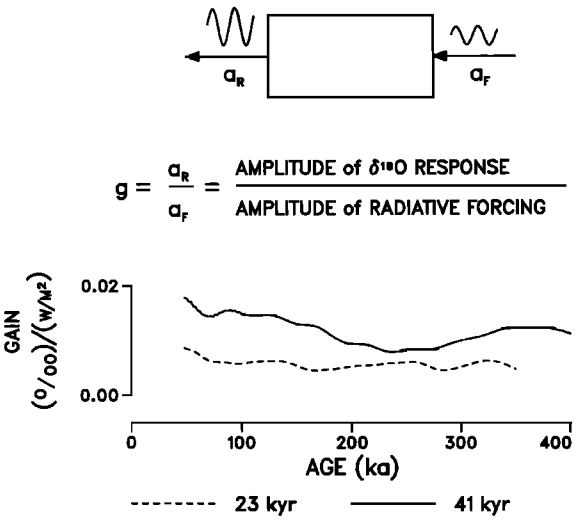

Fig. 9. Gain as a function of time in the precession and obliquity bands. Using the amplitude of the radiation signal at June 65°N in a given band as a measure of the forcing and using the amplitude of the corresponding $\delta^{18}O$ signal as a measure of the system's response, smoothed estimates of the system's gain are obtained from the envelopes in Figure 8. Values have remained fairly constant, the gain at 41 kyr being generally twice that at 23 kyr.

duced by the responses to precession and obliquity. We start by partitioning the $\delta^{18}O$ record into two components: a linear response to Milankovitch forcing and a residual (Figure 10). The linear component is the sum of 23- and 41-kyr responses obtained by digital filtering (Part 1, Figure 9). The residual component, which for brevity we will refer to as the "nonlinear component," is the sum of all variations that are not linearly related to the precession and obliquity forcing.

6.3. *Components of Other Climate Records*

Our next objective is to partition the 11 local climate records examined in this paper into their linear and nonlinear components. In Part 1 we describe each of these time series in some detail. Here we provide a map (Figure 11) and in Figure 12 display three time series that play important roles in our model of the 100-kyr cycle: SST at 44°S (variable 7), SST at 50°N (variable 5), and a deepwater $\Delta\delta^{13}C$ record from the southern hemisphere (variable 20). Using the procedure shown in Figure 10, we now partition these time series into linear and nonlinear components (Figure 13*a* and *c*). As with $\delta^{18}O$, the nonlinear components of the local climate variables are dominated by 100-kyr cycles. These cycles range widely in phase with respect to ice volume and (not surprisingly) exhibit the same phase sequence that we obtained from cross spectra (Figures 4 and 5). The combined linear responses to the two Milankovitch forcings (Figure 13*c*) display the same phase sequence as the nonlinear responses (Figure 13*a*). However,

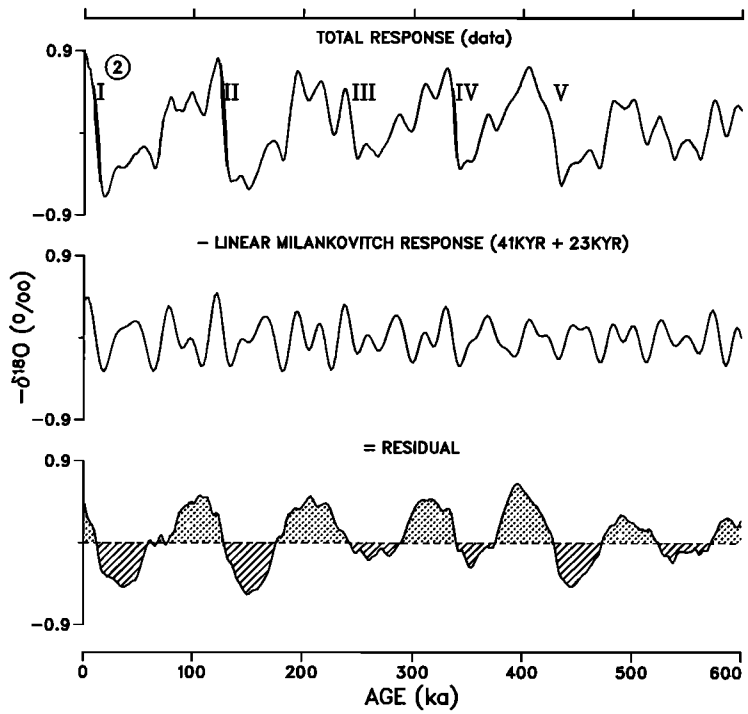

Fig. 10. Partitioning the $\delta^{18}O$ record into two components: a linear response to Milankovitch forcing and a residual. The linear component is the sum of the individual 23- and 41-kyr responses obtained by digital filtering. The residual, nonlinear component is the sum of all variations which are not linearly related to the precession and obliquity forcing. Roman numerals designate terminations of five major glaciations.

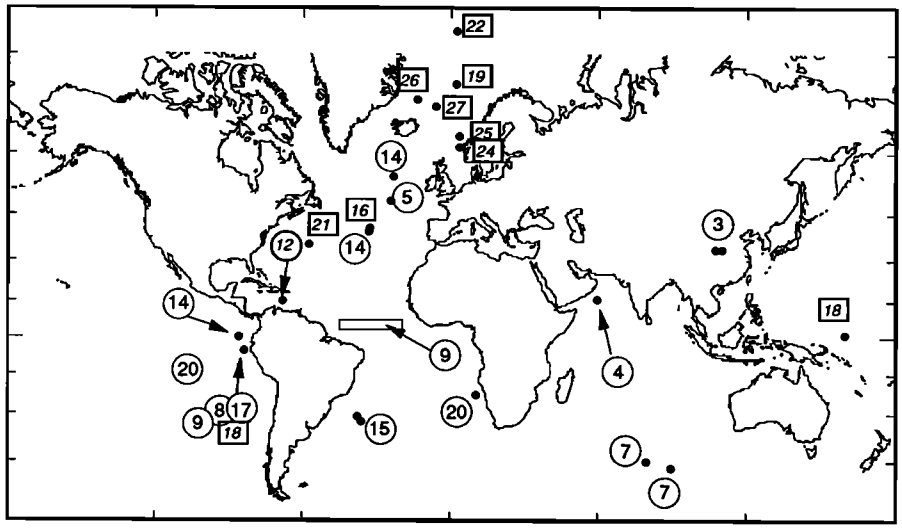

Fig. 11. Location of climate proxy time series. A repeated site number indicates that individual records have been combined by patching, stacking, or differencing to form a single climatic index (Table 1). Open circles indicate long records (~400 kyr). Open squares indicate short, high-resolution records (10 to 200 kyr).

the spectra of the nonlinear (residual) components of variables 5, 7, and 20 (Figure 13*d*) exhibit significant concentrations of variance at frequencies well above the Milankovitch band, including small peaks near 10 kyr. Conceivably, these might reflect the cyclic process identified by Heinrich [1988] in North Atlantic sediments and shown by Bond et al. [1993] to consist of warm-cold oscillations with recurrence times ranging from 10 to 15 kyr. Our $\delta^{18}O$ spectrum is flat in this region, owing in part to the stacking procedure designed to smooth out local effects.

Using the procedure shown in Figure 10, we have partitioned all long time series investigated in this paper into their linear and nonlinear components. To simplify display, we have chosen to present a set of curves obtained by processing the original time series with a band-pass filter (described in Part 1, Figure 8) centered at 100 kyr (Figure 14). In effect,

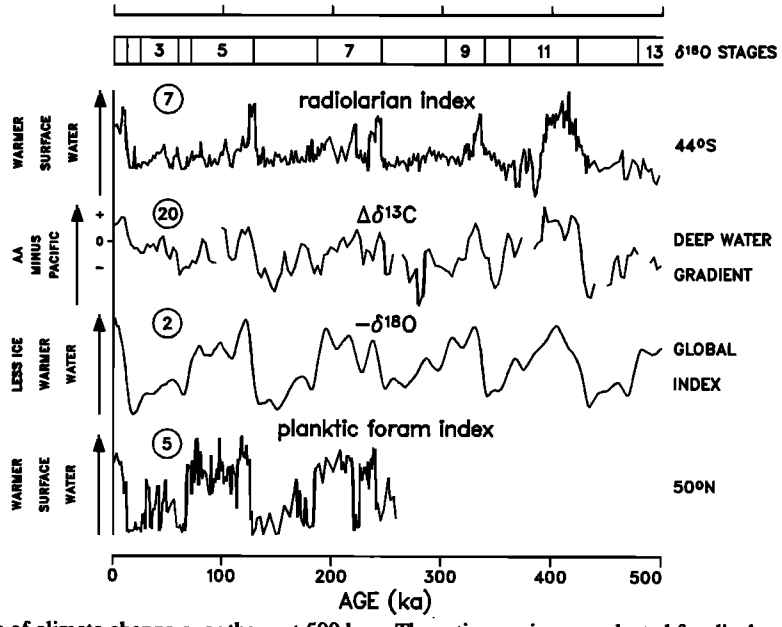

Fig. 12. Patterns of climate change over the past 500 kyr. These time series are selected for display, because they monitor system parameters that play important roles in our model of the 100-kyr cycle, namely, the position of high-latitude ocean fronts, the carbon chemistry of deep waters, and global ice volume. As in Imbrie et al. [1992], we have reversed the signs of observations as needed to give each curve a positive upward sense of change toward an interglacial condition. For curve 20, for example, an upward shift means that deep waters in the Antarctic are becoming more enriched than in the Pacific.

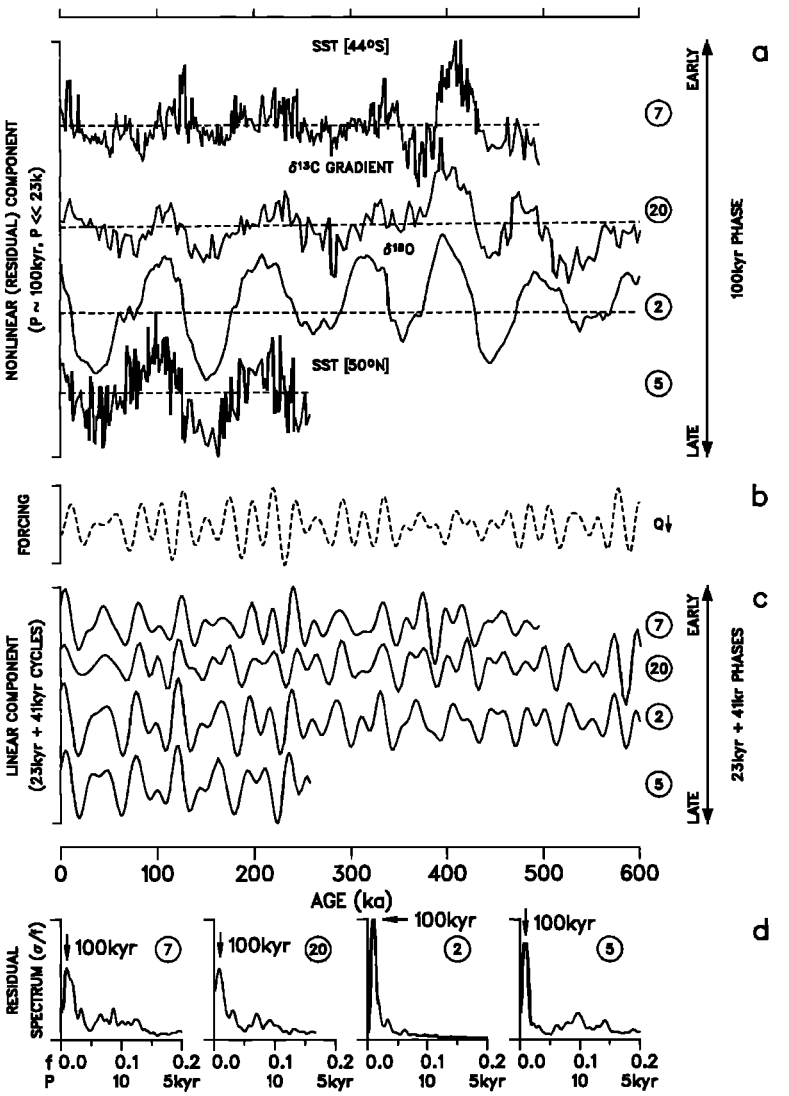

Fig. 13. Comparison of the linear and nonlinear components of four climate records. Each record in Figure 12 has been analyzed into linear and nonlinear components by the procedure shown in Figure 10. (*a*) The 100-kyr oscillations that dominate these nonlinear components display phases that range from early to late with respect to $\delta^{18}O$ (-47° and -35° for variables 7 and 20 respectively; +6° for variable 5). (*b*) Radiation at June 65°N [Berger and Loutre, 1991]. (*c*) The combined linear responses to Milankovitch forcing display the same phase sequence as the nonlinear responses. (*d*) Spectra of nonlinear components of the SST and $\Delta\delta^{13}C$ records exhibit significant variation at frequencies well above the Milankovitch band, including small peaks near 10 kyr.

these curves are smoothed versions of the nonlinear components. Lines drawn with a slope of 360°/100 kyr through the downward zero-crossings of $\delta^{18}O$ show that this train of oscillations progresses systematically through the system with respect to the local changes in $\delta^{18}O$ that are used to align the records (Part 1, Figure 5). When the filtered data are phase-aligned and superposed, the set of oscillations is seen to be mutually coherent.

To help place this phase information in a stratigraphic context, we show in Figure 14 the first derivative of $\delta^{18}O$, that is, the position in the 100-kyr cycle that marks the maximum rate of ice melting. One time series shown in this figure (variable 18) contains important information about Pacific deepwater temperature. In Figure 6 of Part 1, we show how these observations compare with other patterns of climate change over the past 150 kyr. Because this record is too short to be filtered, we plot the smoothed data on Figure 14 and estimate the phase in the 100-kyr band (-58°) by means of a cross spectrum against $\delta^{18}O$. In this way we obtain a very rough estimate of the phase of an important element in the global heat budget. (See also Broecker and Denton [1989, Figure 3]). Significantly, this is precisely the phase our system model estimates for the internal thermal forcing of the 100-kyr cycle (Figure 7 and Table 4). Although the estimate obviously has large un-

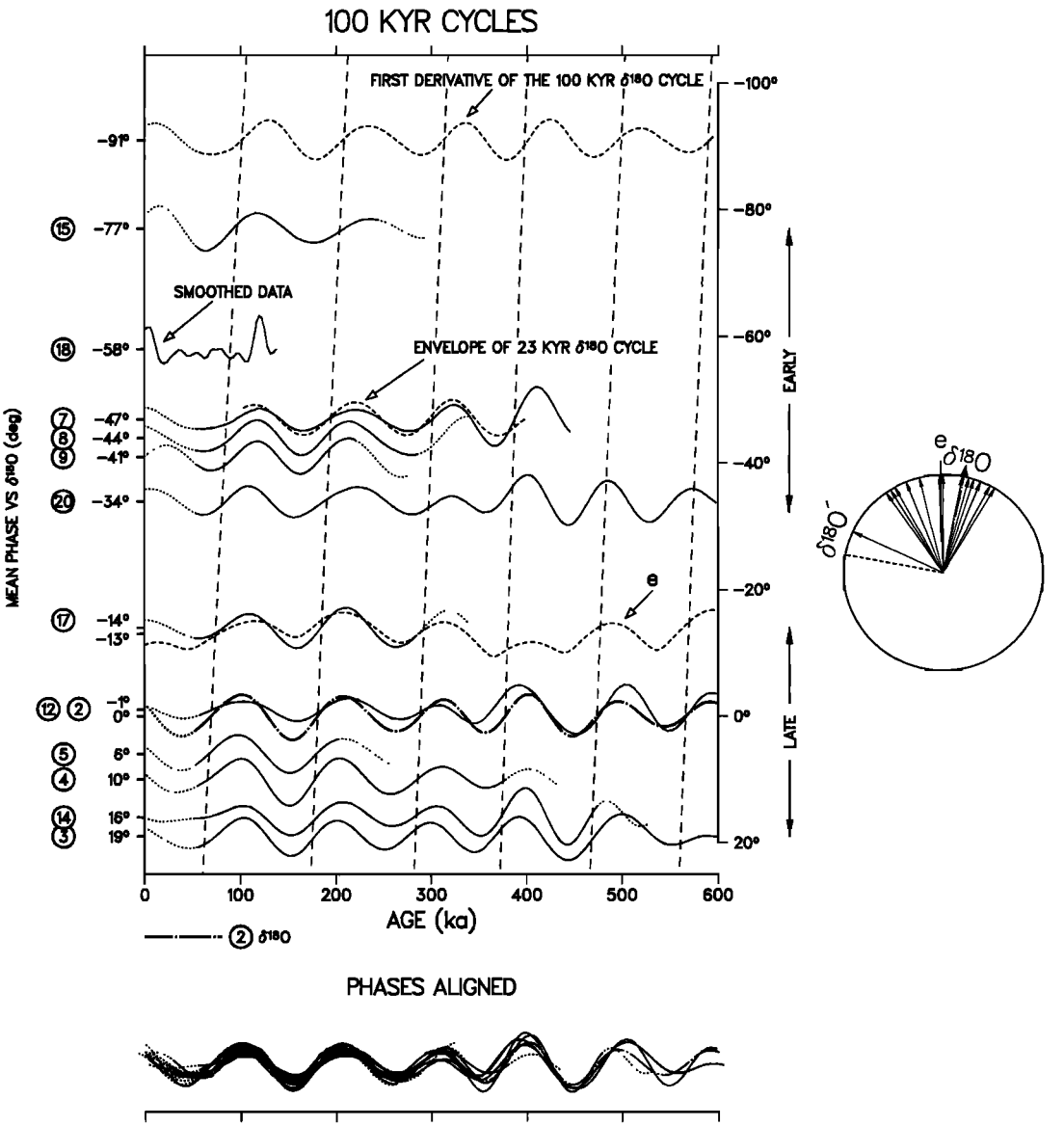

Fig. 14. Sequence of 100-kyr climate cycles. The 100-kyr component of each time series is extracted with a band-pass filter, normalized, and placed on the y axis according to the phase difference (in degrees) with respect to $\delta^{18}O$ (number 2). In effect, the curves based on geological data are smoothed versions of nonlinear components like those shown in Figure 13*a*. Lines drawn with a slope of 360°/100 kyr show that the local climatic responses (Table 1) progress systematically through the system with respect to the local changes in $\delta^{18}O$ that are used to align the records (Part 1, Figure 5). In the phase wheel (right), climate variables are plotted with respect to the maximum of the 100-kyr eccentricity cycle *e* [Berger, 1978*a*, *b*]. The position of $\delta^{18}O$ and its first derivative (dashed line) mark a quadrant of the 100-kyr sea level cycle that starts with maximum melting and ends with maximum sea level.

certainties owing to the short record length, we believe the calculation does support a link between the concept of internal thermal forcing developed in the context of our phase model (section 5.4.1) and the concept of a shift in the mode of ocean circulation developed by Broecker and Denton [1989].

Figure 14 also shows the filtered, 100-kyr component of the upper envelope of the 23-kyr $\delta^{18}O$ cycle (Figure 8*b*). The phase of this envelope indicates that the maximum amplitude of the 23-kyr $\delta^{18}O$ cycle occurs ahead of eccentricity and early in the sequence of climatic responses (~47°). This suggests how a systematic interaction might occur between the 23- and 100-kyr cycles. The highest sea levels in the 23-kyr sea level cycle must occur at or near the maxima in this envelope. Thus, averaged over many cycles, the most rapid and extensive rises in the 23-kyr sea level curve will coincide with times when the 100-kyr sea level curve is approaching its maximum.

In section 7.3.2 we suggest that the combination of these two cyclic patterns yields a condition which, by fostering destruction of ice sheets grounded on continental shelves, would influence the phase of the 100-kyr cycle.

7. A PROCESS MODEL OF THE 100-kyr CYCLE

7.1. *A Two-Million-Year Perspective*

To examine the origin of the 100-kyr cycle, we first look at a two-million-year, high-resolution benthic $\delta^{18}O$ record (Figure 3). The chronology of the older part was obtained by orbital tuning of data from an eastern equatorial Pacific site, Ocean Drilling Program (ODP) 677 [Shackleton et al., 1990]. This timescale has since been verified at two key points by radiometric dating of magnetic reversals [Baksi et al., 1992; Tauxe et al., 1992]. Dominance of the 100-kyr cycle began shortly after one million years ago, a transition seen also in other climatic records that are displayed on the same chronology (e.g., North Atlantic SST and $CaCO_3$ [Ruddiman et al., 1989], South American vegetation [Hooghiemstra and Melice, 1993], and Chinese soils [Kukla et al., 1990]). The transition to this new regime required about 0.3 m.y. Significantly, the variance increase in ODP 677 occurred mainly as an enrichment of $\delta^{18}O$ values during the glacial phase of each cycle. The fact that an isotopic enrichment of about the same magnitude occurred in both the planktonic and benthic records at the same site [Shackleton et al., 1990] suggests that the onset of the 100-kyr cycle regime coincided with an increase in the size of northern hemisphere ice sheets. Thus the isotopic evidence for the onset of a regime with larger ice sheets confirms the same inference made earlier from observations of ice-rafted detritus in a three-core, north-south transect of North Atlantic cores [Ruddiman et al., 1986*a*]. At glacial extremes between about 1 Ma and 0.8 Ma, this debris is found much farther south than previously. This observation implies that a southward shift of the polar front, and therefore of the southern margin of the great ice sheets [Keffer et al., 1988], marked the onset of the 100-kyr regime.

Another important feature of the benthic foraminiferal $\delta^{18}O$ record in Figure 3 is evidence that the system has evolved differently in the three frequency bands where variance is concentrated. In contrast to the 100-kyr cycle, the 23- and 41-kyr cycles have been significant features of climate for the past two million years. And despite the fact that the amplitudes of the 23- and 41-kyr radiation cycles were essentially constant over the entire interval [Berger and Loutre, 1991], the 23- and 41-kyr climate cycles evolved quite differently. After 1 Ma, the strength of the 23-kyr cycle increased, while that of the 41-kyr cycle gradually declined [Imbrie et al., 1993*a*].

What caused the amplitude of the 100-kyr cycle to increase about one million years ago? We suggest that part of the answer lies in the ocean—specifically, in the increased ability of the deep ocean to trap and release carbon in response to glacial-interglacial changes in the export of North Atlantic Deep Water (NADW) [Raymo et al., 1990]. Why this should be so is a problem beyond the scope of this paper, in which we aim only to understand how the 100-kyr cycle has been driven over the past 400 kyr. One possibility is that the Tibetan Plateau, which gradually increased its height during the late Cenozoic, eventually reached a critical elevation that forced long-wave patterns of atmospheric flow favoring the production of NADW [Ruddiman and Kutzbach, 1989].

The problem of explaining the onset of the 100-kyr cycle, and how this event might be related to the passing of thresholds in long-term tectonic and climatic trends, has been addressed in a number of studies [Ruddiman et al., 1989; Saltzman and Maasch, 1990; Raymo, 1992; Saltzman and Verbitsky, 1993]. In one way or another, these studies link the growth of large ice sheets to a global cooling trend, long recognized as a major feature of Earth history during the past 40 million years [Savin et al., 1975; Miller et al., 1987; Crowley and North, 1991]. We consider it likely that this trend is driven by uplift of the Tibetan Plateau and by the positive feedbacks this trend must have initiated, including increases in chemical weathering that gradually lowered the atmospheric concentration of CO_2 [Raymo et al., 1988; Raymo and Ruddiman, 1992].

Long-term trends seen in three of our carbon-system proxies (Part 1, Figure 7, variables 13, 14, 15) show that the mean chemical state of the ocean has continued to evolve over the past half-million years.

7.2. *The Influence of Large Ice Sheets*

The evidence from $\delta^{18}O$ and ice-rafted detritus just presented indicates that the onset of the 100-kyr cycle regime coincided with the appearance of large northern hemisphere ice sheets. This finding agrees with theoretical studies showing that the essential condition for developing a 100-kyr cycle in a time-dependent model is the existence of northern hemisphere ice sheets large enough to exert a strong influence on global climate and sluggish enough to pace key feedbacks of a long-period oscillation (section 4.3). It also confirms the inference we drew from our phase spectra that the 100-kyr cycle exhibits significantly more inertia than the 23- and 41-kyr cycles (section 5.4.2). Our model of the 100-kyr cycle therefore emphasizes two important roles that large ice sheets play in climate dynamics. First, they influence the spatial pattern of climate by controlling the timing of atmospheric and oceanic feedbacks [Ruddiman et al., 1986*b*]. Second, an instability in their response to a rising sea level increases the rate of climate change during deglaciation.

The impact ice sheets have on the atmosphere has been evaluated by equilibrium experiments with general circulation models in which the only prescribed boundary condition change was the insertion of large (last glacial maximum) ice sheets into standard models [Manabe and Broccoli, 1985; Broccoli and Manabe, 1987]. The resulting changes in model climate are confined almost exclusively to the northern hemisphere. In areas never covered by ice, zonal mean temperatures north of 50°N cool by 6°-10°C. In winter, the troposphere has a split flow that straddles the North American ice sheet, the northern branch funneling extremely cold air over the Labrador Sea and downwind across the Atlantic [Kutzbach, 1987; Cooperative Holocene Mapping Project (COHMAP) Members, 1988]. Here sea ice forms and mean temperatures drop by as much as 20°C. Westerly flow in midlatitudes is strengthened from eastern North America across southern Europe and into central Asia, with increased precipitation falling mainly as

snow along a storm track that skirts the southeastern corner of the Laurentide ice sheet and the southern edge of the Scandinavian ice sheet. This part of the response, extrapolated to a time-dependent model, would constitute a positive feedback. The overall effect of the ice sheets on northern hemisphere hydrology is to reduce the mean rate of precipitation by 18%. This might act as a negative feedback, although some experiments with time-dependent models suggest otherwise [Gallée et al., 1992]. Thus the ice budgets for both major ice sheets in these experiments show a negative mass balance, and decreases in soil moisture occur in a zone located just south of both ice sheets. Moreover, the balance of precipitation minus evaporation in the Nordic Sea shifts in favor of more evaporation in response to the increased flow of cold, dry air and other conditions associated with a full glacial state. These elements in the hydrologic response to a large ice sheet would also constitute a negative feedback.

The behavior of any portion of an ice sheet during deglaciation depends crucially on its location. The key point is that parts of large polar ice sheets may be grounded on isostatically depressed continental shelves. In contrast to ice sheets based on land, these marine-based ice sheets are inherently unstable [Mercer, 1968; Weertman, 1974]. This is because grounding lines of the ice streams that drain the ice sheets can retreat rapidly behind low sills during deglaciation. When mechanical thresholds are passed during an interval when sea level is slowly rising as a response to slow ice sheet wasting, significant portions of a particular ice sheet can disintegrate rapidly by shedding icebergs into the ocean [Hughes, 1987]. Although the West Antarctic ice sheet is the only modern example of a marine ice sheet, at the last glacial maximum, ice sheets of this kind certainly occurred around Antarctica [Anderson and Thomas, 1991], occupied the Barents Sea [Solheim et al., 1990], and may well have existed in other parts of the northern continental shelf of Eurasia and North America [Grosswald, 1980; Denton and Hughes, 1981].

7.3. *The 100-kyr Cycle*

7.3.1. *Driving mechanisms.* In Part 1 we present a simple conceptual model of the internal mechanisms that drive each of the Milankovitch glaciation cycles forward (Part 1, Figure 3). This model is "generic" in the sense that the inferred sequence of responses will occur whenever an initial change in the freshwater budget of the Arctic Ocean and Nordic Sea is specified, and for whatever reason that initial change occurs. The model is also generic in the sense that the large amplitude and related special features of the 100-kyr cycle are ignored.

What drives the 100-kyr cycle? Having already concluded that the 100-kyr insolation signal is much too small (and its phase too late) to be a significant cause, we must look for an answer elsewhere. We find our answer in the dynamics of large ice sheets and in the influence these masses of ice exert on the rest of the climate system. Whenever the combination of 23- and 41-kyr cycles forces the size of ice sheets to depart too far from equilibrium, the ice sheets themselves trigger mechanisms that channel climatic energy into the 100-kyr band. The key feedback here is between ice elevation and ice accumulation rate (section 4). By changing the planetary albedo and steering and altering the properties of the winds, large ice sheets in our model force a chain of atmospheric and oceanic responses which, apart from being larger and paced by the inertia of large ice sheets, mimic many features of the externally forced responses.

For example, during the interglacial phase of each 100-kyr ice volume cycle, winds over the North Atlantic force warm, saline, surface water into the Nordic Sea, whereas during the glacial phase, ice sheets force a zonal wind pattern that tends to keep these warm waters out of the Nordic Sea and to bring polar air in contact with larger areas of the North Atlantic. Thus the influence exerted by large ice sheets is quite similar in at least one important way to the influence exerted by radiation in the precession and obliquity bands. In both cases, the flux of heat to the southern ocean is altered by changes in the density of surface waters in the North Atlantic and in the Nordic Sea. As outlined in Part 1, this alteration leads eventually (in our model) to a redistribution of carbon among ocean reservoirs, with global consequences for atmospheric CO_2 in all three cycles.

7.3.2. *Pacing mechanisms and ice sheet size.* Once the growth of large ice sheets becomes possible, owing to the evolution of appropriate boundary conditions, positive feedbacks [Birchfield and Weertman, 1983; Le Treut and Ghil, 1983; Budd and Smith, 1987] are free to amplify the externally forced ice sheet response until it is damped by negative feedbacks [Le Treut and Ghil, 1983; Manabe and Broccoli, 1985; Gallée et al., 1992]. The dynamics of ice-sheet growth will control how long it takes for that limit to be reached and therefore influence both the amplitude and periodicity of glaciation. In section 5.3 we show that the process of growth and decay is well described by a time constant of 15 kyr. In a system so sluggish, linear responses to precession and obliquity forcing must be quite modest (Figure 15). During the 11.5-kyr growth phase of a precession cycle, for example, the actual response an ice sheet would have in response to a step change in forcing is only 53% of its equilibrium response. For the longer, obliquity cycle the response would still be only 64%. But during the 50-kyr growth time of a 100-kyr cycle, 96% of the equilibrium response would be achieved, leaving very little gain if the forcing were continued.

7.3.3. *Deglaciation.* Near the glacial maximum of each

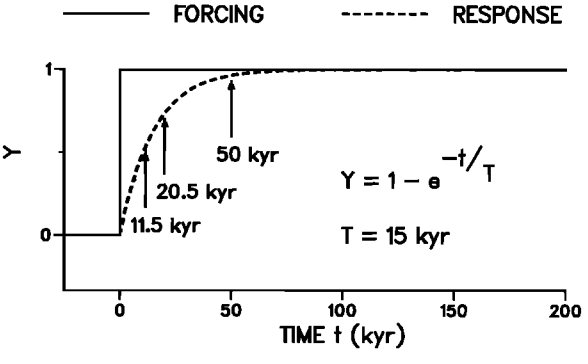

Fig. 15. Response of an ice sheet with a 15-kyr time constant to a step change in the forcing. Designated values of t are the characteristic times [Oerlemans, 1991] of major glaciation cycles.

100-kyr cycle in our model, large portions of polar ice sheets become grounded on isostatically depressed continental shelves in the Barents Sea, in other sectors of the northern polar ocean, and around Antarctica. The mechanical instability of this situation sets the stage for a rapid deglaciation the next time a relatively slow, linearly forced trend of rising sea level crosses a threshold (section 7.2). Late in Stage 2 we have strong evidence in the form of a light $\delta^{18}O$ "spike" to show that such an event did occur in the Barents Sea [Part 1, Figure 13; Jones and Keigwin, 1988; Lehman and Keigwin, 1992*a*].

During some deglaciations it seems likely that the underlying Milankovitch deglacial trend would be reinforced by internal mechanisms acting independently of orbital influences and at higher frequencies. Studies of modern tropical climate make it clear that interactions occur between processes having timescales of the order of 2 years and 3 to 7 years and the annual cycle [Barnett, 1991], and it would not be surprising to find similar interactions operating on geological timescales as well. An examination of high-resolution records of Terminations I and II supports this idea (section 8.1.1 and 8.1.3). An obvious example of an internal process interacting with the Milankovitch trend is a climatic oscillation that has a timescale of several millennia. This process includes the train of Dansgaard-Oeschger events documented in Greenland ice [Dansgaard et al., 1993] and the Younger Dryas oscillation [Berger, 1990]. Another example is the train of North Atlantic cooling cycles known as Heinrich events. These have recurrence times ranging from 10 to 15 kyr [Bond et al., 1993].

We now review evidence that the rising sea level trend, which apparently triggered the deglaciation in the North Atlantic sector, was orbitally forced. The set of ^{14}C-dated observations shown in Figure 16 supports this concept. During the late glacial regime, time series recording the rise of sea level and the retreat of the southern margin of the Laurentide ice sheet are strongly coherent with the radiation curve (dotted area). Over this interval, climate lagged radiation by several

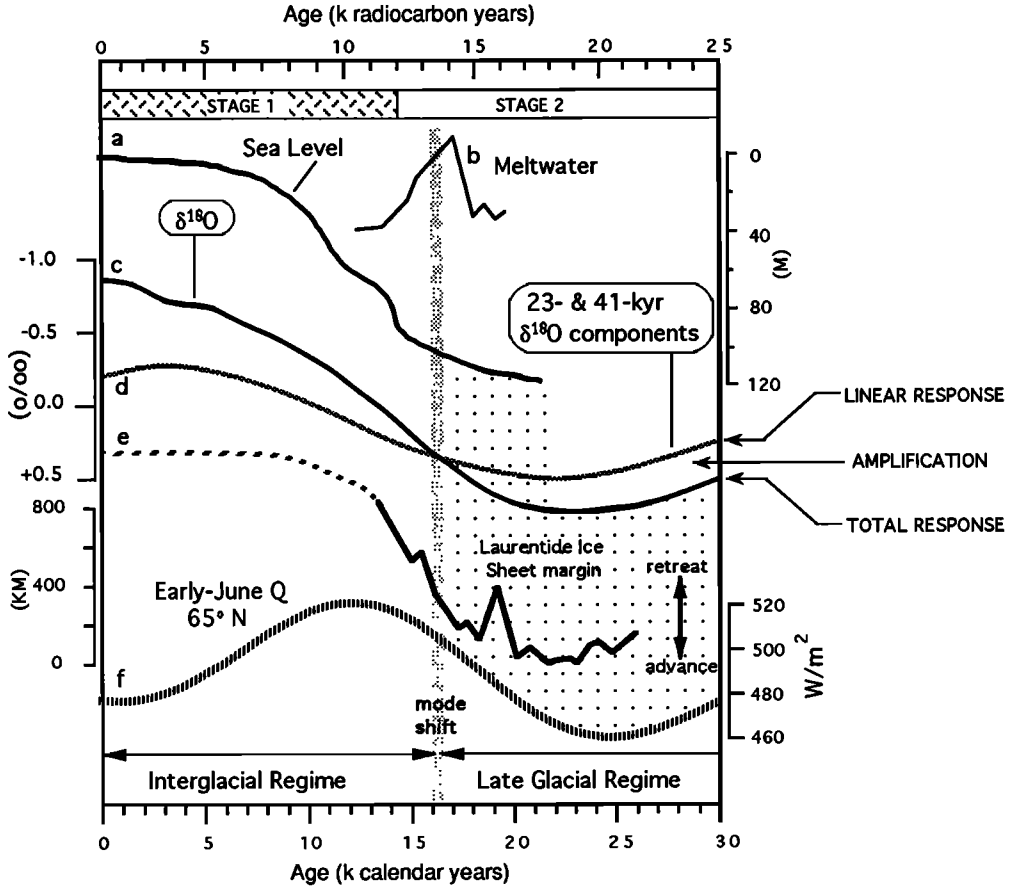

Fig. 16. Evidence that northern hemisphere deglaciation at the end of the last ice age was a response to orbital forcing. Curve a represents the eustatic sea level record from Barbados corals [Fairbanks, 1989]. Curve b represents the $\delta^{18}O$ record of a meltwater event in the Nordic Sea [Jones, 1991]. Curves c and d are $\delta^{18}O$ curves, the calendar-year versions of time series in Figure 10. The transformation is made necessary by the fact that this part of the chronology of Imbrie et al. [1984] is ^{14}C-controlled. The solid segment of curve e shows the observed position of the southern margin of the Miami Sublobe of the Laurentide ice sheet [Broecker and Denton, 1989]; dashed segment shows the pattern we infer for the final retreat. Curve f represents the incoming early June radiation at 65°N [Berger, 1978*a*, *b*]. The ^{14}C-based chronologies of curves a through e have been converted to calendar years with a calibration provided by E. Bard (personal communication, 1992) and based on data in Bard et al. [1993].

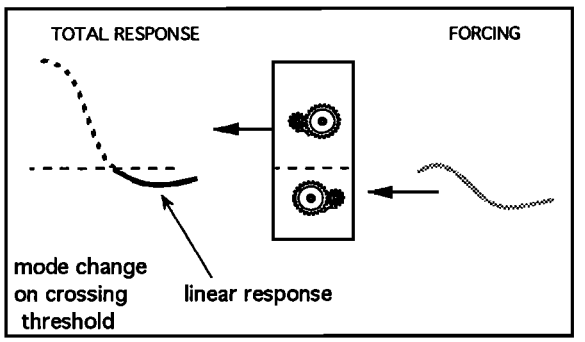

Fig. 17. Model of a nonlinear amplification mechanism. The system's gain is sharply increased when the linear response to an external forcing crosses a threshold.

thousand years. But around 16 kyr B.P., after the ice margin had retreated ~300 km and sea level had risen ~20 m, the climatic responses began to break out of this coherent pattern. The ice margin then began to retreat decisively back from the range of positions it had occupied during late glacial times, setting the stage some 2000 years later for the rapid decay of ice sheets that is recorded by the steepest part of the sea level curve [Fairbanks, 1989].

7.3.4. *Mode shifts.* The pattern of responses shown in Figure 16 is consistent with the view that the immediate cause of rapid changes marking the termination of the Stage 2 glaciation was a reorganization of the ocean-atmosphere system [Broecker and Denton, 1989]. The oceanic part of the reorganization involves a change in the mode of ocean overturning. The pace of deglaciation increases after this mode shift as more heat is pumped into the glaciated regions around the North Atlantic [Lehman and Keigwin, 1992*b*]. An increase in CO_2 that is linked to this change in ocean circulation acts as a strong positive feedback. We conclude that the shift in circulation mode, which in our model is triggered by changes in the Nordic Sea, acts as a nonlinear amplifier on the linearly forced Milankovitch responses (Figure 17). In this way a substantial fraction of the system's internal energy is channeled into the 100-kyr band.

In Figures 3 and 4 of Part 1 we expand the definition of circulation modes given by Broecker and Denton [1989]. In our model, each mode is identified with a particular combination of pathways in the Atlantic's warm-to-cold-water conversion process. These pathways are open ocean convection in the boreal Atlantic (the "boreal heat pump") and the overflow of Nordic intermediate waters (the "Nordic heat pump"). A two-pump mode occurs whenever the exchange between surface waters of the North Atlantic and the Nordic Sea increases sufficiently to produce the overflows that form the core of lower NADW at the same time that deep convection occurs in the open boreal Atlantic. As shown in Figure 18, we assume that a shift from a one-pump to a two-pump mode occurred at Terminations I and II (and at other major deglaciations over the past 400 kyr).

To tie the historical pattern of mode shifts shown in Figure

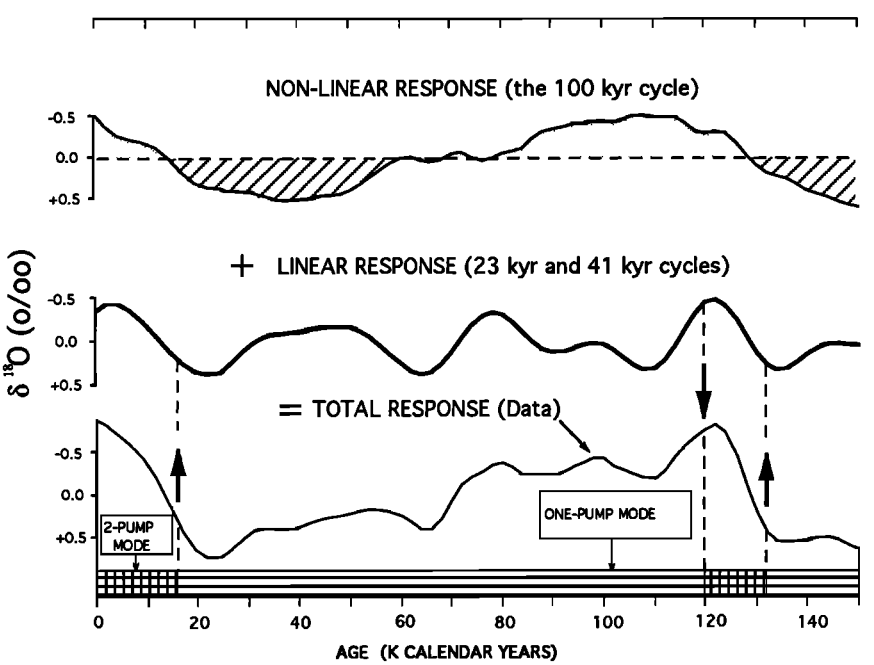

Fig. 18. Inferred circulation modes during the past 150 kyr. The curves are based on time series shown in Figure 10, with a calendar-year correction applied where the dating is ^{14}C-controlled. We suggest that the mode of ocean overturning is determined by the geography of the cold-to-warm-water conversion process that drives the North Atlantic heat pump (Part 1, section 3). The two main branches of this flow are referred to as the boreal heat pump (convection in the open boreal Atlantic) and the Nordic heat pump (overflow of Nordic intermediate waters). At times, the Nordic pump is turned off, leading to a one-pump mode of overturning. Note that the system has a strong linear response while in this mode; the interval of glacial growth between 80 and 60 ka is a linearly forced response, not a mode shift.

18 into our model of the 100-kyr cycle, we return to the concept of an internal thermal forcing (ITF) introduced in section 5.4.1. In section 6.3, we present evidence linking ITF with observations on deep-ocean temperature that reflect the ocean's circulation mode. On this interpretation, the phase of ITF shown in Figure 7 corresponds also to the phase of oceanic mode shifts.

8. DISCUSSION

Our model of processes governing the glaciation cycles includes assumptions about mechanisms operating at two places in the ocean where we lack long time series. One of these is in the Nordic Sea. In this critical region we postulate, first, that there are significant variations in the production of overflow waters and, second, that these oceanic variations occur either as a direct response to Milankovitch forcing or as an indirect response induced by a change in ice sheets. The other place where we lack long time series is the deeper part of the western Atlantic Basin, where heat export linked to the deep overflow is concentrated in the modern ocean [Reid and Lynn, 1971; Lehman and Keigwin, 1992*a*, *b*] .

In this section we use available data to test two aspects of the model's performance at specific times in the climate narrative: its prediction of the sequence of system responses within the two critical areas just discussed and its prediction that climate will lag early June radiation at 65°N. In section 8.1.1 we examine an independent, ^{14}C-dated set of high-resolution data over the past 25,000 years. In the three sections that follow we use the common temporal framework provided by $\delta^{18}O$ to examine the sequence of system responses during four intervals of major change that lie beyond the range of ^{14}C (Stage 4, the onset and termination of glaciations flanking Stage 5e, and the termination of the Stage 12 glaciation). As discussed in section 4.1 of Part 1, the precision of this correlation framework has an average uncertainty of the order of ±2.5 kyr. The average uncertainty of the absolute ages in this framework is estimated to be ±5 kyr. Unfortunately, only a limited number of independent observations are now available to us for intervals older than 25 ka: a Cd/Ca proxy for deep ventilation (variable 16), and several measures of conditions in the Nordic Sea obtained from cores 19 and 27.

8.1. *Testing the Model at Specific Places and Times*

8.1.1. *Termination of the Stage 2 glaciation.* How well do the nature and timing of events compare with our model? To make a valid comparison between geological observations dated by ^{14}C and an astronomically based radiation curve, it is necessary to convert ^{14}C years into calendar years [Stuiver et al., 1991]. For this we use a calibration provided by E. Bard (personal communication, 1992) that is based on the data of Bard et al. [1990] and Bard et al. [1993]. Given a ^{14}C age in kiloyears C, the calendar age is $1.39\ C - 0.0056\ C^2 - 1.81$, where $6 < C \leq 25$. The display in Figure 19 (like that in Figure 16) confirms our expectation that an increase in Arctic insolation (curve h) precedes a sequence of oceanic responses that begins with a change in the character of surface waters in the Nordic Sea and ends with a change in the deep Atlantic. After the initial local deglaciation recorded (by curve d) as a brief meltwater event (ND), the blooming of diatoms (curve e) and the entry of Atlantic foraminifera into the eastern Norwegian Sea (record i) signal an increased exchange of saline Atlantic water (IE). We infer that the resulting increase in the production of overflow water culminated ~16 kyr B.P. in a decisive increase in the ventilation of the deep Atlantic, as recorded in our phosphate proxies (curves f and g). Some 9 kyr later, the deglaciation process culminated in the demise of the Laurentide ice sheet. Although the dating of the first decisive increase in CO_2 (curve a) is not yet well constrained, the currently accepted chronology of this event [Leuenberger et al., 1992] is consistent with our expectation that it would follow shortly after an increase in deep NADW export.

The details of the deep-ventilation time series (curve g), taken from Keigwin et al. [1991], show a pattern that might represent a damped oscillation (with a recurrence time of ~2 kyr) superposed on the underlying deglacial trend. Like these authors, we take this as evidence supporting the idea that a train of thermohaline oscillations was triggered by meltwaters from glaciated areas surrounding the North Atlantic [Birchfield and Broecker, 1990; Broecker et al., 1990]. An oscillating response of this type is dynamically consistent with our finding (Figure 6) that a delay of 1 kyr occurs in the system's initial response [Bhattacharya et al., 1982]. Such a delay has the potential for initiating an oscillation with a recurrence time of the order of 2 kyr [Ghil et al., 1987; Wright et al., 1990]. Similar oscillations also seem to characterize older deglaciations [Sarnthein and Tiedemann, 1990].

Another interesting feature of the data in Figure 19 is that once the system has been forced into an interglacial state, there is considerable resistance to the Milankovitch forcing toward a glacial state. Only one time series in this figure can be interpreted as a precursor of glaciation. This is the decrease in relative abundance of Atlantic diatoms in the Iceland Sea (curve c) and an increase (not shown) of diatoms that are characteristic of polar waters [Karpuz and Schrader, 1990]. These trends in the phytoplankton suggest that the maximum exchange (ME) between Atlantic and Nordic Sea waters occurred around 7 kyr B.P. Under this interpretation, the decreasing exchange since then implies a lowering salinity that would favor a return to a one-pump circulation mode.

8.1.2. *Onset of the Stage 4 glaciation.* The transition from Stage 5 to Stage 4 is defined by a relatively rapid shift in the $\delta^{18}O$ curve that implies a rapid interval of ice growth (Figure 20). At this climatic turning point, as at Termination I, there is no doubt that the change in ice volume (curve b) lags radiation (curve a). One feature of special interest in this figure is the demonstration that variable 5 (SST at 50°N) and variable 14 (deepwater $\Delta\delta^{13}C$ ventilation index at 41°N) both lag slightly behind $\delta^{18}O$. This pattern is in agreement with our phase observations (Figure 5) that place variables 5 and 14 in the group of late (R_4) responses—responses we take to be driven by the wind field and therefore linked to the extent of the northern hemisphere ice sheets. Moreover, the Cd/Ca proxy for deep ventilation (variable 16), which has too short a record to be included in our phase analysis, is seen here to be essentially on phase with the $\Delta\delta^{13}C$ ventilation proxy (variable 14).

8.1.3. *Glaciations flanking Stage 5e.* Geological records of events leading to and following the Stage 5e interglacial provide a unique opportunity to discover not only how a glacial age ends, but how one begins [Kukla and Went, 1992].

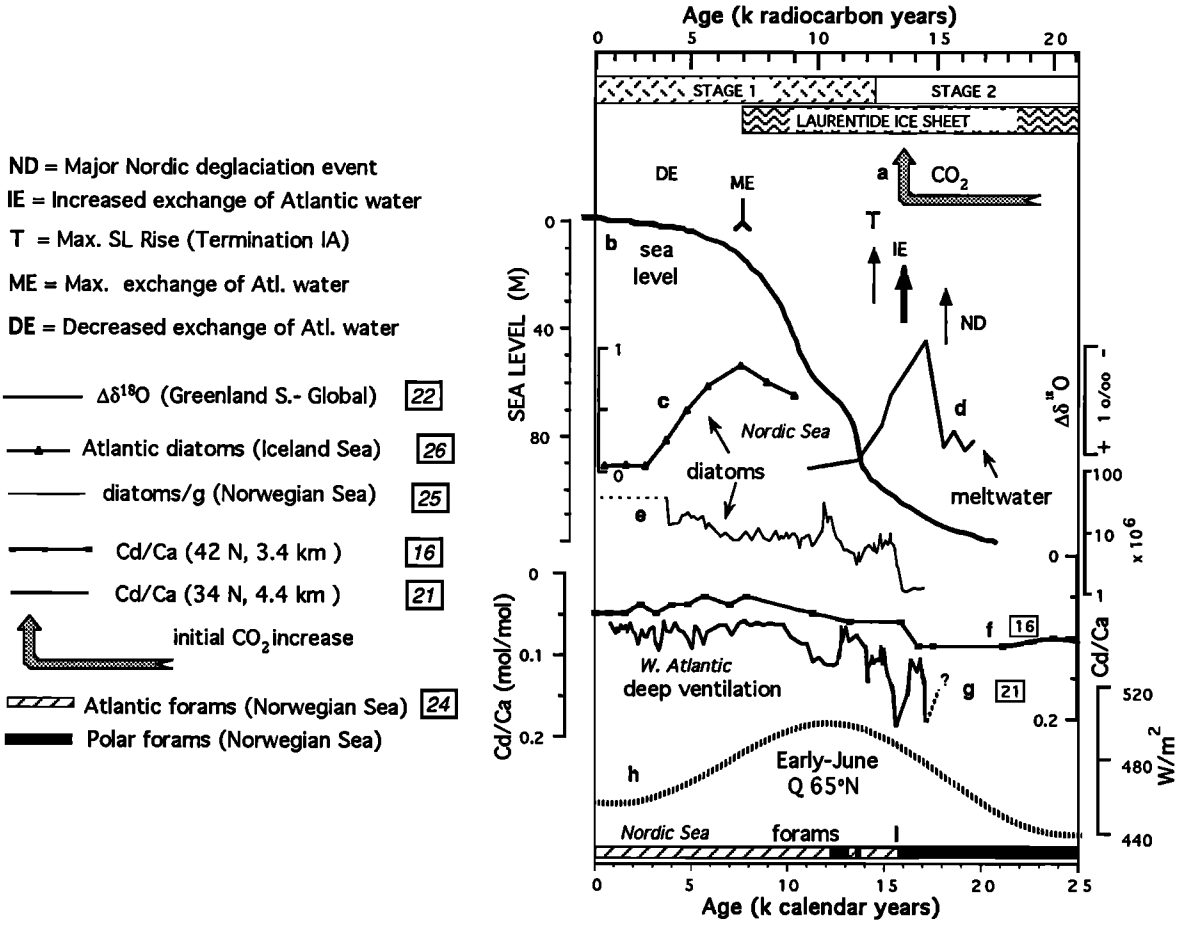

Fig. 19. Changes in the surface waters of the Nordic Sea and deep North Atlantic during termination of the Stage 2 glaciation. Curve a is from Leuenberger et al. [1992], curve b from Fairbanks [1989], and curve c represents a diatom assemblage from Karpuz and Schrader [1990]. Curve d represents the Greenland Sea $\delta^{18}O$ minus global $\delta^{18}O$ [Jones, 1991], curve e indicates diatoms per gram of sediment from Karpuz and Jansen [1992]. Curve f is from Boyle and Keigwin [1985], curve g from Keigwin et al. [1991], curve h from Berger [1978*a*, *b*] and record i from Lehman and Keigwin [1992*b*]. The ^{14}C-based chronologies (curves b-g and record i) have been converted to calendar years with a calibration provided by E. Bard (personal communication, 1992) and based on data from Bard et al. [1993]. Figure 11 and Table 1 locate the cores (identified in numbered boxes).

Before examining some of the evidence (Figure 21) it will be useful to review our basis for correlating and dating these time series. Unlike the time series examined in section 8.1.1, whose absolute chronologies are controlled by ^{14}C, the chronologies for six curves shown in Figure 21 (curves a through f) have been developed by correlating the $\delta^{18}O$ in each core against the standard SPECMAP $\delta^{18}O$ chronology (curve b). As discussed previously, this procedure gives information on the sequence of events that is essentially independent of any absolute chronology that may be adopted. The precision of these correlations, expressed as a time difference between two deep-sea cores from the open ocean, averages about ±3 kyr over a string of closely spaced observations. However, where observations are widely spaced, as they are in several records chosen for analysis here (because they provide crucial but hard-to-get information about these sites), the precision of the correlation is degraded. Thus in displaying curves a and h, we show the possible range of correlations during the deglaciation. This is not done with curve d, because the point to be made is simply that a foraminiferal species typical of the open Atlantic, *G. bulloides*, occurs in the Nordic Sea for only a short interval during Stage 5e. This conclusion is well documented in other records which sample this interval in more detail [Kellogg et al., 1978].

Because information about CO_2 displayed in Figure 21 (curve h) is derived from an Antarctic ice core, the problem of correlating that record with marine $\delta^{18}O$ poses a different and very challenging stratigraphic problem. The correlation shown in Figure 21 is taken from Sowers et al. [1991], who base their correlation on observations of $\delta^{18}O$ in air bubbles in the Vostok core.

One other important matter remains to be considered,

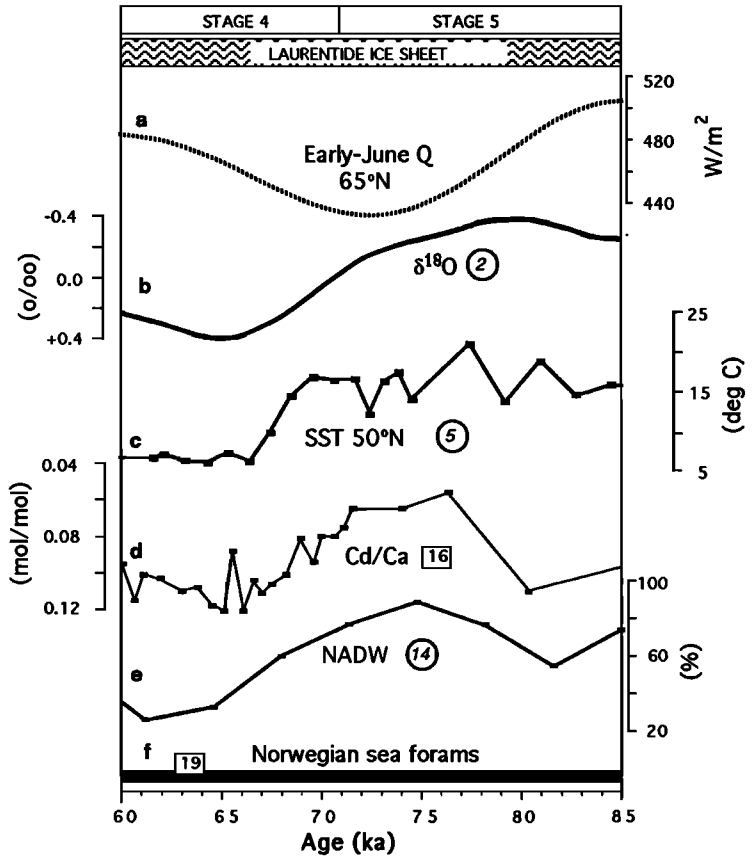

Fig. 20. Changes in the surface and deep North Atlantic during the Stage 4 interval of rapid glacial growth. Curve a represents early June insolation [Berger, 1978*a*, *b*]. Curve b is the SPECMAP $\delta^{18}O$ stack [Imbrie et al. 1984], curve c the foraminiferal index of SST in K708-1 [Ruddiman and McIntyre, 1984], curve d is the Cd/Ca proxy for phosphate concentration [Boyle and Keigwin, 1985; Imbrie et al., 1992], curve e the $\Delta\delta^{13}C$ measure of the contribution of northern sources to North Atlantic Deep Water [Raymo et al., 1990], and record f the foraminiferal assemblage in core K-11 [Kellogg et al., 1978]. Symbols are as in Figure 19. See text for a discussion of the precision and accuracy of the common temporal framework provided by $\delta^{18}O$ stratigraphy (sections 3.2.3 and 8.2.1).

namely the accuracy of age estimates for the marine records shown in Figure 21. These estimates are those of the SPECMAP chronology. In our view, the true ages are probably as stated, within ±5 kyr for individual points and within ±3 kyr for the average of a long string of points. This view finds some support in a chronology recently developed for the Vostok ice core and in the correlation of that record with the marine $\delta^{18}O$ record via the $\delta^{18}O$ composition of air bubbles trapped in the ice [Jouzel et al., 1993]. However, other investigators [Lambeck and Nakada, 1992; Winograd et al., 1992] argue that the SPECMAP ages for events near Termination II are too young by some 15 kyr. As we proceed to draw climatic conclusions from the information in Figure 21, therefore, we must keep in mind these differences of opinion about the absolute accuracy of the dating. In this section we will assume that the SPECMAP chronology is correct. In the next section we will examine the consequences for theories of the 100-kyr cycle if the true ages of events late in Stage 6.2 prove to be considerably older than the ages assigned in the SPECMAP timescale [Imbrie et al., 1984; Martinson et al., 1987].

Viewed on the SPECMAP chronology, the data in Figure 21 generally confirm the predictions of our model. For the glacial termination, a sequence of events in the Nordic Sea that is broadly similar to the sequence near the end of Stage 2 (Figure 19) occurred near the end of Stage 6. An increase in radiation (Figure 21, curve g) led a local deglaciation event (ND) recorded locally by $\Delta\delta^{18}O$ (curve a), which in turn led the main termination (T) as recorded by a shift in the global $\delta^{18}O$ stack (curve b). The termination clearly lagged not only radiation but also lagged an increase in Atlantic foraminifera (record i). This suggests that an increase in the exchange of saline Atlantic water (IE) turned on the Nordic pump, as in our model. But owing to uncertainties in correlating records from the Nordic Sea and from the Vostok ice core with the $\delta^{18}O$ stack, it is not possible to conclude that event ND or IE actually led the increase in CO_2 [Sowers et al., 1991].

The idea that the precise timing of a particular termination

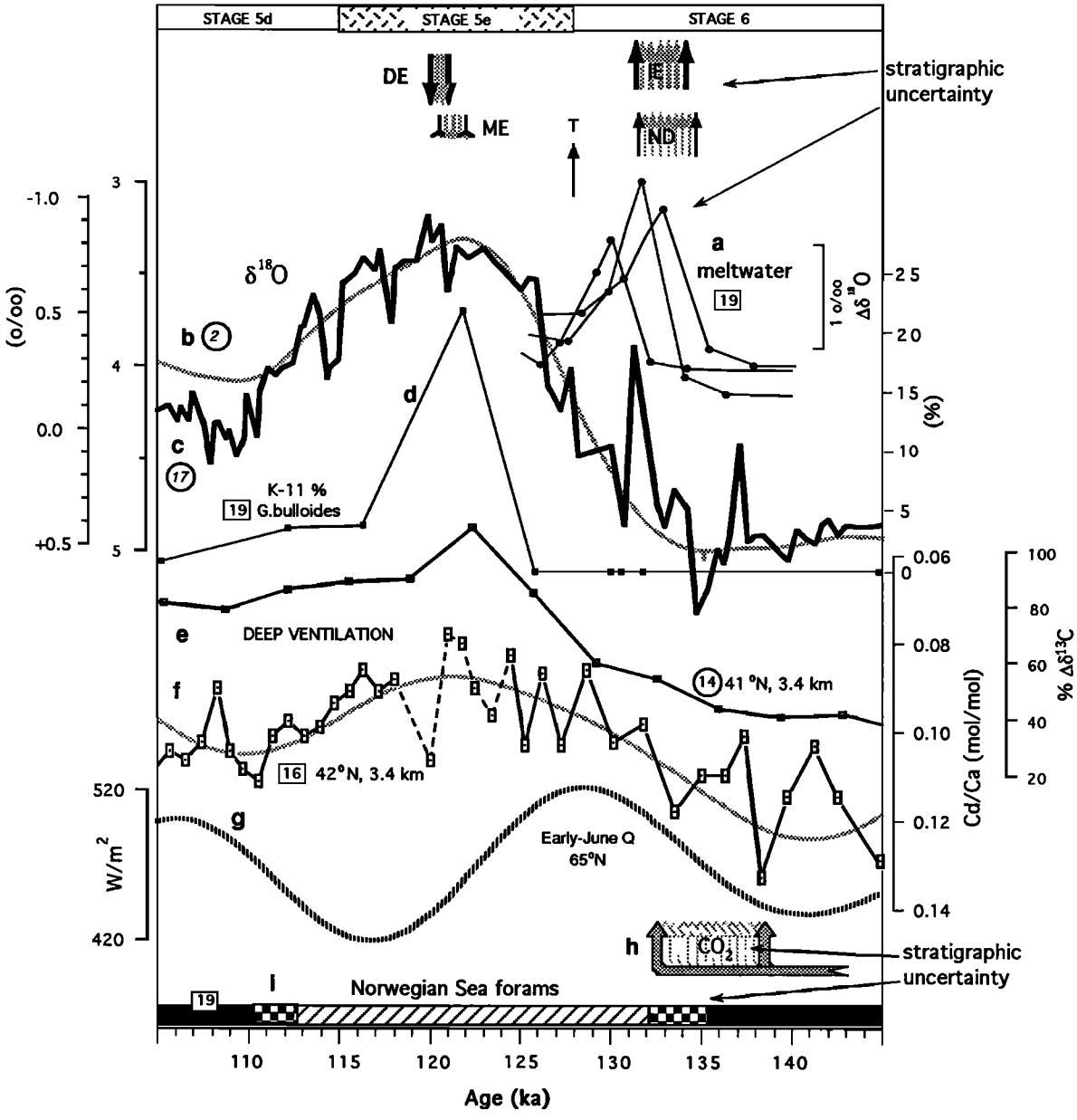

Fig. 21. Changes in the surface waters of the Nordic Sea and deep North Atlantic during the termination and onset of glaciations flanking the penultimate interglacial (Stage 5e). Curves a show the possible stratigraphic range of a salinity index derived from the planktonic $\delta^{18}O$ in Norwegian Sea core K-11 [Kellogg et al., 1978] by subtracting the global $\delta^{18}O$ stack. Curve b is the SPECMAP planktonic $\delta^{18}O$ stack, curve c the benthic $\delta^{18}O$ in V19-30 [Shackleton and Pisias, 1985], curve d the percentage of *G. bulloides* in core K-11, curve e the $\Delta\delta^{13}C$ measure of the contribution of northern sources to NADW [Raymo et al., 1990], and curve f the Cd/Ca proxy for phosphate concentration [Boyle and Keigwin, 1985; Imbrie et al., 1992]. The underlying trend in curve f (shaded curve) is derived by filtering the entire 220-kyr record (Part 1, Figure 6). Note that the Cd/Ca value recorded at the 5e peak has been compromised by reworking so that the true Cd/Ca minimum may not be recorded. Curve g shows early June insolation [Berger, 1978*a*, *b*], curve h represents the increase in CO_2 [Sowers et al., 1991], and record i shows foraminiferal assemblages in core K-11 [Kellogg et al., 1978]. Symbols are as in Figure 19. See text for a discussion of the precision and accuracy of the common temporal framework provided by $\delta^{18}O$ stratigraphy (sections 3.2.3 and 8.2.1).

might be influenced not only by an underlying Milankovitch trend but also by events reflecting an internal oscillation that occurs independently of this trend and at a higher frequency (section 7.3.3) is supported by two conspicuous light spikes in the high-resolution $\delta^{18}O$ record (curve c). The larger spike, peaking around 132 ka, might correlate both with the meltwater event in the Greenland Sea (curve a) and with the onset of the first major warm interval in the Greenland summit ice core, that is, the interval designated MIS-5e5 by the Greenland Ice-Core Project Members [1993].

Late in Stage 5e, during the earliest phase of glacier growth recorded by $\delta^{18}O$, a species of Atlantic foraminifera that today is characteristic of the open North Atlantic diminished in abundance (curve d). This decline was followed by the loss of all foraminifera characteristic of the modern open Atlantic (record i). We take this as evidence that a decreasing exchange of Atlantic water (DE) following the maximum exchange (ME) led to a decrease in salinity which turned off the Nordic pump, as in our model. As expected, these events lag the initial decline of radiation.

Close examination of the phase relationships between our deepwater ventilation proxies (curves e and f) and $\delta^{18}O$ (curves b and c) is instructive. Late in Stage 6, these ventilation measures slightly lead $\delta^{18}O$, whereas they are essentially in phase from the $\delta^{18}O$ minimum of Stage 5e through Stage 5d. In late Stage 5 and Stage 4, the same ventilation measures lag $\delta^{18}O$ (Figure 20), thus exhibiting there the average phase relationship seen in cross spectra. We conclude that the lagging pattern, which was apparently typical during the moderate glaciation conditions of Stages 4 and 5d, dominates in the long-term average over the in-phase or leading patterns that are apparently typical only of full glacials.

8.1.4. *Termination of the Stage 12 glaciation.* From a Milankovitch perspective, the deglaciation which terminated the maximum glaciation of Stage 12 and led to full interglacial conditions of Stage 11 is one of the major ice age puzzles (Figure 12). As noted in section 3, the essence of the puzzle is a mismatch between the amplitude of Stage 11 and the amplitude of the insolation change associated with it (Figure 2). Figure 10 provides an opportunity to evaluate this mismatch by comparing the amplitude of the linear response to insolation with the amplitude of the total response. The linear response associated with Termination V is, in fact, the smallest of any termination. Two other unique features of this termination are worth noting: its long duration and the presence of a conspicuous shoulder on the $\delta^{18}O$ curve. These features can be seen in more detail in Figure 22, which is plotted with the same scaling as Figures 19-21. Unfortunately, records 5 (Atlantic SST at 50°N) and 16 (deep Atlantic Cd/Ca ventilation index at 42°N) are not long enough to be included in this figure. But the information we do have shows that the timing of two low-amplitude features in the insolation record (curve c) is broadly consistent with a Milankovitch interpretation of similar features in $\delta^{18}O$ (curve a) and deep ventilation (curve b). Moreover, the sudden increase in Norwegian Sea foraminifera (record d) indicates that as predicted by our model, the shift to interglacial conditions was led by an increase in the flow of saline Atlantic waters into the Nordic Sea.

8.1.5. *Summary.* Although encouraged by the results of these limited tests, we regard it as important to obtain longer and more detailed observations from the deep basin of the western Atlantic (near site 16). As discussed next, it is also important to obtain more accurate dates for oceanic events that occurred late in Stage 6.

8.2. *Alternate Explanations*

Our review of major theories (section 4.3) concludes that the most likely explanation for the late Pleistocene 100-kyr glaciation cycle lies between two end-member models. The first is a self-sustaining, internal oscillation paced by the large time constant of large ice sheets. Here external forcing plays no role. The second end-member explains the cycle as a nonlinear response to orbital forcing. In this case, the phase is set by the attainment of a threshold in the system's response. In principle, the crossing of this threshold might be caused in two ways: (1) by the externally forced responses acting alone ("simple external pacing") or (2) by the externally forced responses acting in combination with an internally driven, higher-frequency process ("mixed pacing"). In the latter case, the Milankovitch response may be said to condition the system so that the relatively small-amplitude output of some internal process is sufficient to trigger a major deglaciation.

8.2.1. *Observations.* In principle, it should be possible to choose between these models by comparing the timing and amplitude of the insolation forcing with our knowledge of climate history. Toward this end we now review the evidence for the major climatic turning points presented in section 8.1, with particular attention to unresolved questions of chronology.

1. One of these turning points occurred during the last major deglaciation, about 16,000 calendar years ago (Figure 19). Here there is no doubt that the ^{14}C-dated observations are consistent with the idea that both the deglaciation and the system's shift to a different circulation mode were responses to a Milankovitch forcing. However, one coincidence of orbital and climatic events does not prove the case for this deglaciation or demonstrate that other deglaciations were caused in the same way.

2. Another turning point was the rapid growth of ice sheets in Stage 4, an interval where no serious doubts have been expressed about the accuracy of the SPECMAP chronology. Here the evidence not only supports the idea of a Milankovitch response (Figure 20), but indicates that the ice-volume response is essentially linear (Figure 18). This orbitally forced onset of a new climatic regime that is marked by larger ice sheets seems to set the North Atlantic stage for a series of Heinrich oscillations [Bond et al., 1993].

3. Two major climatic turning points flank the penultimate interglacial (Figure 21). One of these is the onset of glaciation which began late in Stage 5e. According to the chronology adopted in this paper, this event (like the two just discussed) also lags the insolation forcing. The other climatic turning point is the major deglaciation known as Termination II. Here again, on the chronology adopted in this paper, the climate change recorded by global and local $\delta^{18}O$ curves lags the insolation forcing. Taken at face value, then, our chronology of these events also supports the Milankovitch response model.

However, a universally accepted chronology for Termina-

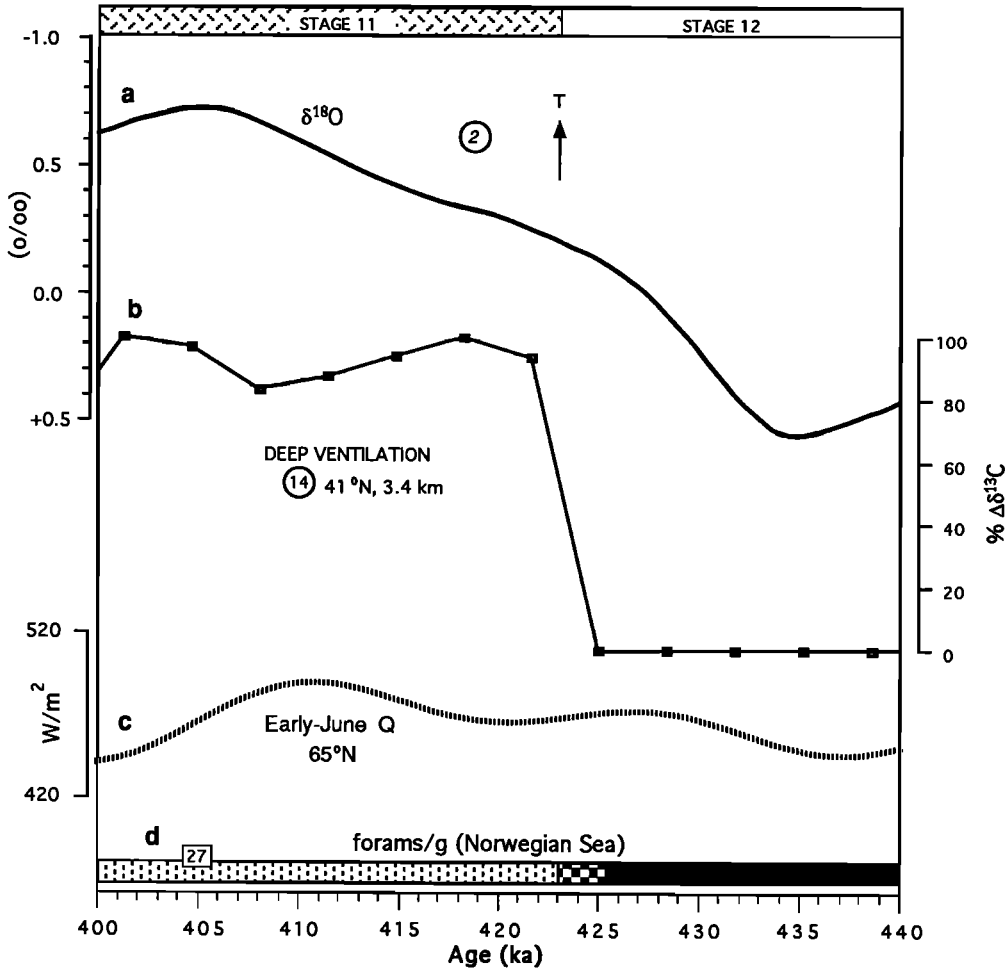

Fig. 22. Changes in the surface waters of the Nordic Sea and deep North Atlantic during the termination of the Stage 12 glaciation. Curve a is the SPECMAP $\delta^{18}O$ stack, curve b the $\Delta\delta^{13}C$ measure of the contribution of northern sources to NADW [Raymo et al., 1990], curve c early-June insolation [Berger, 1978 *a*, *b*], and record d shows the number of planktonic foraminifera per gram in core V28-56 (<1000 = solid; >10,000 = dashed) [Kellogg et al., 1978]. Other symbols are as in Figure 19. See text for a discussion of the precision and accuracy of the common temporal framework provided by $\delta^{18}O$ stratigraphy (sections 3.2.3 and 8.2.1).

tion II is not yet available [Bard et al., 1991; Hamelin et al., 1991]. Some studies have suggested the possibility that the sea level rise might have taken place before the radiation minimum that occurred at 141 ka. Lambeck and Nakada [1992] draw this conclusion from a revised isostatic rebound model, while Winograd et al. [1992] base their views on studies of a groundwater $\delta^{18}O$ record from Devils Hole, Nevada. Moreover, there remains considerable uncertainty about the timing of the CO_2 increase relative to the changes in sea level and marine $\delta^{18}O$ [Sowers et al., 1991]. To help choose among alternative explanations, therefore, we need a more precise knowledge of the correlation [Turon, 1984] as well as the timing of these events. If, for example, the date for a decisive shift of the $\delta^{18}O$ record out of Stage 6 (135 ±5 ka in the SPECMAP chronology) should prove to be older than 140 ka and therefore close to or older than the radiation minimum at 141 ka, this finding would support the "mixed pacing" model discussed above. If, on the other hand, the date of this turnaround should remain within the stated uncertainty limits, the finding would support the "simple external pacing" model.

Recently, two groups of investigators have developed (or improved previously existing) chronologies for polar ice cores in Greenland and Antarctica [Dansgaard et al. 1993; Jouzel et al., 1993]. These chronologies, obtained independently of the SPECMAP age model, support our view that the deglaciation which ended the penultimate (Stage 6) glaciation was orbitally forced by the increase in radiation that began about 141 ka. Assuming that both the ice core and SPECMAP chronologies are correct, we find that as expected, the local air-temperature response occurs first, followed by the global ice volume changes recorded by oceanic $\delta^{18}O$.

4. Finally, we consider the termination of the Stage 12 glaciation. Unlike the termination of the Stage 6 glaciation, the date for this event (Termination V) is essentially the same

on the SPECMAP and Devils Hole chronologies: the heaviest oceanic $\delta^{18}O$ values occur in Stage 12 and the lightest values in the corresponding part of the Devils Hole record occur at about 435 ka. The associated minimum in early June radiation at 65°N precedes that date by 2 kyr. The potential theoretical problem here is not with the dating of this event, which fits the Milankovitch forcing model reasonably well, but with its amplitude. This is the "Stage 11 problem" identified in Figure 2. The total amplitude of the linear response to the orbital forcing (Figure 10) is quite small compared to the amplitude of the 100-kyr response. In particular, the ratio between forcing and response is much smaller than it is for Termination I. However, since the model developed in this paper depends not on the total range of the linear response that triggers a mode shift, but only on the early part of the (sea level) response that triggers the marine ice sheet instability, there may be no fundamental difficulty in accepting the Milankovitch forcing model. Time-dependent modeling experiments over the interval in question should shed light on this problem.

8.2.2. *Modeling experiments.* Conceivably, the climate system has evolved in such a way that at different times in Earth history, a different balance of internal and external mechanisms is responsible for setting the phase of a particular 100-kyr oscillation. Given the complexity of the system, we think it unlikely that acquisition of new data alone will suffice to determine how important a contribution any particular mechanism makes to any 100-kyr cycle. We need numerical models of candidate mechanisms, especially models that in addition to simulating the global ice volume curve make predictions of the phases of other internal responses so that these predicted sequences can be compared with data [Saltzman and Sutera, 1987; Le Treut et al., 1988].

8.3. *Unexplained Features*

The central feature of our model of the 100-kyr cycle is the influence that large northern hemisphere ice sheets exert on the rest of the climate system. If no other influences were at work, and if the links between ice and climate were linear, we would expect to find a nearly perfect correlation between the 100-kyr cycle of $\delta^{18}O$ and the 100-kyr cycle of every other climate proxy. Not surprisingly, many of the correlations we observe are far from perfect. Thus many important features of climate history remain unexplained by our simple model. As one example, although the long-term NADW record from site 607 (variable 14) shows a general trend toward stronger glacial NADW suppression after 1 Ma, the magnitude of glacial $\delta^{18}O$ events is by no means perfectly correlated with the magnitude of NADW suppressions.

9. CONCLUSIONS

1. For at least the past two million years, cycles of glaciation with periods near 23- and 41-kyr have been forced by anomalies in the pattern of incoming radiation. Within each of these frequency bands, a significant portion of the response to this Milankovitch forcing is linear.

2. About a million years ago, a large-amplitude 100-kyr cycle began to dominate the $\delta^{18}O$ record of glacial variability. But a simple Milankovitch origin of this cycle is ruled out, because the eccentricity-driven 100-kyr radiation cycle is much too small and its phase too late to force the corresponding climate cycle directly.

3. The onset of this regime coincides with the appearance of large northern hemisphere ice sheets. This inference from observations on ice-rafted detritus and $\delta^{18}O$, combined with modeling studies, suggests that large northern hemisphere ice sheets are an essential condition for the development of feedbacks to drive the 100-kyr ice volume cycle. In low latitudes, however, large 100-kyr cycles can be developed independently of large ice sheets.

4. Oceanic changes associated with each of the three major glaciation cycles can be examined in a geographic array of time series that monitor ocean properties over the past 400 kyr. Cross-spectral analysis of this array reveals that the geographic progression of local responses in the 100-kyr cycle is similar to the progression in the other two cycles, implying that a similar set of internal mechanisms operates in all three.

5. Quantitative modeling of the observed phase sequences shows that the 100-kyr cycle requires a source of inertia having a time constant (~15,000 years) much larger than the other cycles (~5000 years). Our conceptual model identifies massive northern hemisphere ice sheets as the larger inertial source which, by pacing interactions with the atmosphere, ocean, and lithosphere, produces the internal thermal forcing that drives the 100-kyr glaciation cycle.

6. In this model, whenever the combination of the 41-kyr and 23-kyr cycles forces the size of the ice sheets to depart too far from equilibrium, the ice sheets themselves drive and pace mechanisms in the atmosphere and ocean that channel climatic energy into the 100-kyr band. By changing the albedo, steering the winds, and altering the properties of air masses in contact with the ocean and land, the growth and decay of ice sheets cause changes in the mode of ocean circulation. These mode shifts amplify the system's initial, modest responses to external forcing by transporting heat to boreal latitudes and by changing the concentration of atmospheric CO_2.

7. When sea level is forced upward from major lows by a Milankovitch response acting either alone, or in combination with an internally driven, higher-frequency process such as the Heinrich oscillation, ice sheets grounded on continental shelves become unstable, mass wasting accelerates, and the resulting deglaciation sets the phase of one wave in the train of 100-kyr oscillations.

8. In this view, the 100-kyr cycle is a response to the Milankovitch forcing in which the coupled air-sea-ice system acts as a nonlinear amplifier. However, from the evidence now in hand we cannot rule out the possibility that a self-sustaining oscillation might also contribute to the strength of this cycle.

9. In any case, when considered over the entire bandwidth of the Milankovitch signal, the climate system exhibits strong nonlinear behavior. It is, nevertheless, possible to construct simple but useful models of this complex behavior by partitioning the total response into the three band-limited cycles.

Acknowledgments. We are grateful to E. Birchfield, W. S. Broecker, T. J. Crowley, R. G. Fairbanks, H. Gallée, M. Ghil, T. Hughes, P. E. Labeyrie, D. Murray, P. E. Olsen, W. R. Peltier, W. F. Ruddiman, and B. Saltzman for constructive

criticism of earlier drafts of this paper; to M. Bender, T. Sowers, and T. F. Stocker for helpful discussions; to E. Bard for providing a calendar calibration of ^{14}C dates; and to A. Broccoli, T. Kellogg, and D. A. Short for providing unpublished data. Much of the work reported here has been supported by a National Science Foundation grant to the multi-institutional SPECMAP project. This support includes SPECMAP grants ATM8812589 to Brown University (Imbrie and Prell), ATM8812640 to Oregon State University (Mix and Pisias), ATM8812637 to the Lamont-Doherty Earth Observatory, Columbia University (Kukla, Martinson, McIntyre), and ATM8812639 to the University of Wisconsin (Kutzbach). We also acknowledge NERC grant GR3/606 (Shackleton) and NSF support from the following grants: ATM8902849 and ATM8713227 to the University of Wisconsin (Kutzbach), OCE8810949 (Raymo) and ATM8703017 (Kukla) to LDEO, OCE8710168 to MIT (Boyle), ATM8706394 (Imbrie) and ATM8516140 (Imbrie and Shackleton, December 1985 to December 1990) to Brown University. A continuation of ATM8516140 (January 1991 through the present) supported the senior author's work on this project. This paper is Lamont-Doherty Earth Observatory contribution no. 5134.

REFERENCES

Anderson, J. B., and M. A. Thomas, Marine ice-sheet decoupling as a mechanism for rapid, episodic sea-level change: The record of such events and their influence on sedimentation, in *The Record of Sea-Level Fluctuations*, vol. 70, edited by K. T. Biddle and W. Schlager, pp. 87-104, Elsevier Science, New York, 1991.

Baksi, A. K., V. Hsu, M. O. McWilliams, and E. Farrar, $^{40}Ar/^{39}Ar$ dating of the Brunhes-Matuyama geomagnetic field reversal, *Science, 256,* 356-357, 1992.

Bard, E., B. Hamelin, R. G. Fairbanks, and A. Zindler, Calibration of the ^{14}C timescale over the past 30,000 years using mass spectrometric U-Th ages from Barbados corals, *Nature, 345,* 405-410, 1990.

Bard, E., R. G. Fairbanks, B. Hamelin, A. Zindler, and C. T. Hoang, Uranium-234 anomalies in corals older than 150,000 years, *Geochim. Cosmochim. Acta, 55,* 2385-2390, 1991.

Bard, E., M. Arnold, R. G. Fairbanks, and B. Hamelin, ^{230}Th-^{234}U and ^{14}C ages obtained by mass spectrometry on corals, *Radiocarbon, 35,* 191-199, 1993.

Barnett, R. P., The interaction of multiple time scales in the tropical climate system, *J. Climate, 4,* 269-285, 1991.

Berger, A., Long-term variations of caloric insolation resulting from the Earth's orbital elements, *Quat. Res., 9,* 139-167, 1978*a*.

Berger, A., *A Simple Algorithm to Compute Long Term Variations of Daily or Monthly Insolation*, 39 pp., Université Catholique de Louvain, Louvain, Belgium, 1978*b*.

Berger, A., and M. F. Loutre, Insolation values for the climate of the last 10 million years, *Quat. Sci. Rev., 10,* 297-317, 1991.

Berger, A., M. F. Loutre, and J. Laskar, Stability of the astronomical frequencies over the Earth's history for paleoclimate studies, *Science, 255,* 560-566, 1992.

Berger, A. L., Insolation signatures of Quaternary climatic changes, *Nuovo Cimento Soc. Ital. Fis., Ser. C, 2,* 63-87, 1979.

Berger, W. H., The Younger Dryas cold spell — A quest for causes, *Palaeogeogr., Palaeoclimatol., Palaeoecol., 89,* 219-237, 1990.

Bhattacharya, K., M. Ghil, and I. L. Vulis, Internal variability of an energy-balance model with delayed albedo effects, *J. Atmos. Sci., 39,* 1747-1773, 1982.

Birchfield, G. E., and W. S. Broecker, A salt oscillator in the glacial Atlantic?, 2, A "scale analysis" model, *Paleoceanography, 5,* 835-843, 1990.

Birchfield, G. E., and M. Ghil, Climate evolution in the Pliocene and Pleistocene from marine-sediment records and simulations: Internal variability versus orbital forcing, *J. Geophys. Res., 98,* 10,385-10,399, 1993.

Birchfield, G. E., and R. W. Grumbine, "Slow" physics of large continental ice sheets and underlying bedrock, and its relation to the Pleistocene ice ages, *J. Geophys. Res, 90,* 11,294-11,302, 1985.

Birchfield, G. E., and J. Weertman, A note on the spectral response of a model continental ice sheet, *J. Geophys. Res., 83,* 4123-4125, 1978.

Birchfield, G. E., and J. Weertman, Topography, albedo-temperature feedback, and climate sensitivity, *Science, 219,* 284-285, 1983.

Bond, G., W. Broecker, S. Johnsen, J. McManus, L. Labeyrie, J. Jouzel, and G. Bonani, Correlations between climate records from North Atlantic sediments and Greenland ice, *Nature, 365,* 143-147, 1993.

Boyle, E. A., Cadmium in benthic foraminifera and abyssal hydrography: Evidence for a 41 kyr obliquity cycle, in *Climate Processes and Climate Sensitivity, Geophys. Monogr. Ser.*, vol. 29, edited by J. E. Hansen and T. Takahashi, pp. 360-368, AGU, Washington, D. C., 1984*a*.

Boyle, E. A., Sampling statistic limitations on benthic foraminifera chemical and isotopic data, *Mar. Geol., 58,* 213-224, 1984*b*.

Boyle, E. A., and L. D. Keigwin, Comparison of Atlantic and Pacific paleochemical records for the last 215,000 years: Changes in deep ocean circulation and chemical inventories, *Earth Planet. Sci. Lett., 76,* 135-150, 1985.

Broccoli, A. J., and S. Manabe, The influence of continental ice, atmospheric CO_2 and land albedo on the climate of the last glacial maximum, *Clim. Dyn., 1,* 87-99, 1987.

Broecker, W. S., and J. van Donk, Insolation changes, ice volumes, and the ^{18}O record in deep-sea cores, *Rev. Geophys., 8,* 169-197, 1970.

Broecker, W. S., and G. H. Denton, The role of ocean-atmosphere reorganizations in glacial cycles, *Geochim. Cosmochim. Acta, 53,* 2465-2501, 1989.

Broecker, W. S., G. Bond, M. Klas, G. Bonani, and W. Wolfli, A salt oscillator in the glacial Atlantic?, 1, The concept, *Paleoceanography, 5,* 469-477, 1990.

Budd, W. F., and I. N. Smith, Conditions for growth and retreat of the Laurentide ice sheet, *Geogr. Phys. Quat., 41,* 279-290, 1987.

Calder, N., Arithmetic of ice ages, *Nature, 252,* 216-218, 1974.

Clemens, S. C., and W. L. Prell, Late Pleistocene variability of Arabian Sea summer monsoon winds and continental aridity: Eolian records from the lithogenic component of deep-sea sediments, *Paleoceanography, 5*, 109-145, 1990.

Clemens, S. C., and W. L. Prell, Late Quaternary forcing of Indian Ocean summer-monsoon winds: A comparison of Fourier model and general circulation model results, *J. Geophys. Res., 96*, 22,683-22,700, 1991.

Cooperative Holocene Mapping Project (COHMAP) Members, Climatic changes of the last 18,000 years: Observations and model simulations, *Science, 241*, 1043-1052, 1988.

Crowley, T. J., and G. R. North, *Paleoclimatology*, 339 pp., Oxford University Press, New York, 1991.

Crowley, T. J., K.-Y. Kim, J. G. Mengel, and D. A. Short, Modeling 100,000-year climate fluctuations in pre-Pleistocene time series, *Science, 255*, 705-707, 1992.

Curry, W. B., and T. J. Crowley, The $\delta^{13}C$ of equatorial Atlantic surface waters: Implications for ice age pCO_2 levels, *Paleoceanography, 2*, 489-517, 1987.

Dansgaard, W., S. J. Johnsen, H. B. Clausen, D. Dahl-Jensen, N. S. Gundestrup, C. U. Hammer, C. S. Hvidberg, J. P. Steffensen, A. E. Sveinbjörnsdottir, J. Jouzel, and G. Bond, Evidence for general instability of past climates from a 250-kyr ice core record, *Nature, 364*, 218-220, 1993.

DeBlonde, G., and W. R. Peltier, A one-dimensional model of continental ice volume fluctuations through the Pleistocene: Implications for the origin of the mid-Pleistocene climate transition, *J. Clim., 4*, 318-344, 1991.

Denton, G. H., and T. J. Hughes, *The Last Great Ice Sheets*, 484 pp., Wiley-Interscience, New York, 1981.

Fairbanks, R. G., A 17,000-year glacio-eustatic sea level record: Influence of glacial melting rates on the Younger Dryas event and deep-ocean circulation, *Nature, 342*, 637-642, 1989.

Gallée, H., J. P. van Ypersele, T. Fichefet, C. Tricot, and A. Berger, Simulation of the last glacial cycle by a coupled, sectorially averaged climate-ice sheet model, 1, The climate model, *J. Geophys. Res., 96*, 13,139-13,161, 1991.

Gallée, H., J. P. van Ypersele, T. Fichefet, I. Marsiat, C. Tricot, and A. Berger, Simulation of the last glacial cycle by a coupled, sectorially averaged climate-ice sheet model, 2, Response to insolation and CO_2 variation, *J. Geophys. Res., 97*, 15,713-15,740, 1992.

Gallée, H., A. Berger, and N. J. Shackleton, Simulation of the climate of the last 200 kyr with the LLN 2D-Model, in *Ice in the Climate System*, edited by W. R. Peltier, D. Reidel, Norwell, Mass., 1993.

Genthon, C., J. M. Barnola, D. Raynaud, C. Lorius, J. Jouzel, N. I. Barkov, Y. S. Korotkevich, and V. M. Kotlyakov, Vostok ice core: Climatic response to CO_2 and orbital forcing changes over the last 2 climatic cycles, *Nature, 329*, 414-418, 1987.

Ghil, M., Climate sensitivity, energy balance models, and oscillatory climate models, *J. Geophys. Res., 89*, 1280-1284, 1984.

Ghil, M., Deceptively-simple models of climatic change, in *Climate and Geo-sciences*, vol. 285, edited by A. L. Berger et al., pp. 211-240, Kluwer Academic, Norwell, Mass., 1989.

Ghil, M., Quaternary glaciations: Theory and observations, in *The Sun in Time*, edited by C. P. Sonett et al., pp. 511-542, University of Arizona, Tucson, 1991.

Ghil, M., and S. Childress, *Topics in Geophysical Fluid Dynamics: Atmospheric Dynamics, Dynamo Theory and Climate Dynamics*, 485 pp., Springer-Verlag, New York, 1987.

Ghil, M., A. Mullhaupt, and P. Pestiaux, Deep water formation and Quaternary glaciations, *Clim. Dyn., 2*, 1-10, 1987.

Greenland Ice-Core Project Members, Climate instability during the last interglacial period recorded in the GRIP ice core, *Nature, 364*, 203-207, 1993.

Grosswald, M. G., Late Weichselian ice sheet of northern Eurasia, *Quat. Res., 13*, 1-32, 1980.

Hagelberg, T., and N. Pisias, Linear and nonlinear couplings between orbital forcing and the marine $\delta^{18}O$ record during the late Neogene, *Paleoceanography, 6*, 729-746, 1991.

Hamelin, B., E. Bard, A. Zindler, and R. G. Fairbanks, $^{234}U/^{238}U$ mass spectrometry of corals: How accurate is the U-Th age of the last interglacial period?, *Earth Planet. Sci. Lett., 106*, 169-180, 1991.

Hays, J. D., J. Imbrie, and N. J. Shackleton, Variations in the Earth's orbit: Pacemaker of the ice ages, *Science, 194*, 1121-1132, 1976.

Heinrich, H., Origin and consequences of cyclic ice rafting in the Northeast Atlantic Ocean during the past 130,000 years, *Quat. Res., 29*, 142-152, 1988.

Hooghiemstra, H., and J. L. Melice, Pleistocene evolution of orbital periodicities in the high-resolution pollen record Funza I, Eastern Cordillera, Colombia, in *Orbital Forcing and Cyclic Sequences*, edited by P. L. DeBoer and D. G. Smith, Blackwell, Oxford, 1993.

Horel, J. D., On the annual cycle of the tropical Pacific atmosphere and ocean, *Mon. Weather Rev., 11*, 1863-1878, 1982.

Hughes, T., Ice dynamics and deglaciation models when ice sheets collapsed, in *North America and Adjacent Oceans During the Last Deglaciation*, vol. K-3, edited by W. F. Ruddiman and H. E. Wright, Jr., pp. 183-220, Geological Society of America, Boulder, Colorado, 1987.

Imbrie, J., and J. Z. Imbrie, Modeling the climatic response to orbital variations, *Science, 207*, 943-953, 1980.

Imbrie, J., J. D. Hays, D. G. Martinson, A. McIntyre, A. C. Mix, J. J. Morley, N. G. Pisias, W. L. Prell, and N. J. Shackleton, The orbital theory of Pleistocene climate: Support from a revised chronology of the marine $\delta^{18}O$ record, in *Milankovitch and Climate, Part 1*, edited by A. L. Berger et al., pp. 269-305, D. Reidel, Norwell, Mass., 1984.

Imbrie, J., A. McIntyre, and A. Mix, Oceanic response to orbital forcing in the late Quaternary: Observational and experimental strategies, in *Climate and Geo-sciences*, vol. 285, edited by A. Berger et al., pp. 121-164, Kluwer Academic, Norwell, Mass., 1989.

Imbrie, J., E. Boyle, S. Clemens, A. Duffy, W. Howard, G. Kukla, J. Kutzbach, D. Martinson, A. McIntyre, A. Mix, B. Molfino, J. Morley, L. Peterson, N. Pisias, W. Prell, M. Raymo, N. Shackleton, and J. Toggweiler, On the structure and origin of major glaciation cycles, 1, Linear

responses to Milankovitch forcing, *Paleoceanography*, 7. 701-738, 1992.

Imbrie, J., A. Berger, and N. J. Shackleton, Role of orbital forcing: A two-million-year perspective, in *Global Changes in the Perspective of the Past*, edited by J. A. Eddy and H. Oeschger, pp. 263-279, John Wiley, New York, 1993*a*.

Imbrie, J., A. C. Mix, and D. G. Martinson, Milankovitch theory viewed from Devils Hole, *Nature, 363*, 531-533, 1993*b*.

Jenkins, G. M., and D. G. Watts, *Spectral Analysis and Its Applications*, 525 pp., Holden-Day, Oakland, Calif., 1968.

Jones, G. A., Spatial and temporal distribution of Laurentide and Fennoscandian meltwater during the last deglaciation, *Nor. Geol. Tidsskr., 71*, 145-148, 1991.

Jones, G. A., and L. D. Keigwin, Evidence from Fram Strait (78° N) for early deglaciation, *Nature, 336*, 56-59, 1988.

Jouzel, J. et al., Extending the Vostok ice-core record of palaeoclimate to the penultimate glacial period, *Nature, 364*, 407-412, 1993.

Karpuz, N. K., and E. Jansen, A high-resolution diatom record of the last deglaciation from the SE Norwegian Sea: Documentation of rapid climatic changes, *Paleoceanography, 7*, 499-520, 1992.

Karpuz, N. K., and H. Schrader, Surface sediment diatom distribution and Holocene paleotemperature variations in the Greenland, Iceland, and Norwegian Sea, *Paleoceanography, 5*, 557-580, 1990.

Keffer, T., D. G. Martinson, and B. H. Corliss, The position of the Gulf Stream during Quaternary glaciations, *Science, 241*, 440-442, 1988.

Keigwin, L. D., G. A. Jones, S. J. Lehman, and E. A. Boyle, Deglacial meltwater discharge, North Atlantic deep circulation, and abrupt climate change, *J. Geophys. Res., 96*, 16,811-16,828, 1991.

Kellogg, T. B., J.-C. Duplessy, and N. J. Shackleton, Planktonic foraminiferal and oxygen isotopic stratigraphy and paleoclimatology of Norwegian deep-sea cores, *Boreas, 7*, 61-73, 1978.

Kukla, G., Comment on "The Pleistocene epoch and the evolution of man" by C. Emiliani, *Current Anthropology, 9*, 37-39, 1968.

Kukla, G., and J. Gavin, Insolation regime of the warm to cold transitions, in *Start of a Glacial*, vol. 3, edited by G. Kukla and E. Went, pp. 307-339, Springer-Verlag, New York, 1992.

Kukla, G., and E. Went (Eds.), *Start of a Glacial*, 353 pp., Springer-Verlag, New York, 1992.

Kukla, G., A. Berger, R. Lotti, and J. Brown, Orbital signature of interglacials, *Nature, 290*, 295-300, 1981.

Kukla, G., Z. S. An, J. L. Melice, J. Gavin, and J. L. Xiao, Magnetic susceptibility record of Chinese loess, *Trans. R. Soc. Edinburgh Earth Sci., 81*, 263-288, 1990.

Kutzbach, J. E., Model simulations of the climatic patterns during the deglaciation of North America, in *North America and Adjacent Oceans During the Last Deglaciation*, vol. K-3, edited by W. F. Ruddiman and H. E. Wright, Jr., pp. 425-446, Geological Society of America, Boulder, Colo., 1987.

Kutzbach, J. E., and P. J. Guetter, The influence of changing orbital parameters and surface boundary conditions on climate simulations for the past 18,000 years, *J. Atmos. Sci., 43*, 1726-1759, 1986.

Lambeck, K., and M. Nakada, Constraints on the age and duration of the last interglacial period and on sea-level variations, *Nature, 357*, 125-128, 1992.

Lautenschlager, M., and K. Herterich, Atmospheric response to ice age conditions: Climatology near the Earth's surface, *J. Geophys. Res., 95*, 22,547-22,557, 1990.

Lehman, S. J., and L. D. Keigwin, Sudden changes in North Atlantic circulation during the last deglaciation, *Nature, 356*, 757-762, 1992*a*.

Lehman, S. J., and L. D. Keigwin, Deep circulation revisited, *Nature, 358*, 197-198, 1992*b*.

Le Treut, H., and M. Ghil, Orbital forcing, climatic interactions, and glaciation cycles, *J. Geophys. Res., 88*, 5167-5190, 1983.

Le Treut, H., J. Portes, J. Jouzel, and M. Ghil, Isotopic modeling of climatic oscillations: Implications for a comparative study of marine and ice core records, *J. Geophys. Res., 93*, 9365-9383, 1988.

Leuenberger, M., U. Siegenthaler, and C. C. Langway, Carbon isotope composition of atmospheric CO_2 during the last ice age from an Antarctic ice core, *Nature, 357*, 488-490, 1992.

Maasch, K. A., and B. Saltzman, A low-order dynamical model of global climatic variability over the full Pleistocene, *J. Geophys. Res., 95*, 1955-1963, 1990.

Manabe, S., and A. J. Broccoli, The influence of continental ice sheets on the climate of an ice age, *J. Geophys. Res., 90*, 2167-2190, 1985.

Martinson, D. G., N. G. Pisias, J. D. Hays, J. Imbrie, T. C. Moore, and N. J. Shackleton, Age dating and the orbital theory of the ice ages: Development of a high-resolution 0 to 300,000-year chronostratigraphy, *Quat. Res., 27*, 1-30, 1987.

Mercer, J. H., Antarctic ice and Sangamon sea level, in *International Association of Scientific Hydrology, Commission of Snow and Ice*, vol. 79, pp. 217-225, General Assembly of Bern, Bern, 1968.

Meskó, A., *Digital Filtering Applications in Geophysical Exploration for Oil*, 636 pp., John Wiley, New York, 1984.

Mesolella, K. J., R. K. Matthews, W. S. Broecker, and D. L. Thurber, The astronomical theory of climatic change: Barbados data, *J. Geol., 77*, 250-274, 1969.

Milankovitch, M., *Mathematische Klimalehre und Astronomische Theorie der Klimaschwankungen*, 176 pp., Gebruder Borntreger, Berlin, 1930.

Miller, K. G., R. G. Fairbanks, and G. S. Mountain, Tertiary oxygen isotope synthesis, sea level history, and continental margin erosion, *Paleoceanography, 2*, 1-19, 1987.

Mix, A. C., N. G. Pisias, R. Zahn, W. Rugh, C. Lopez, and K. Nelson, Carbon-13 in Pacific deep and intermediate waters, 0-370 ka: Implications for ocean circulation and Pleistocene CO_2, *Paleoceanography, 6*, 205-226, 1991.

Munk, W. H., and D. E. Cartwright, Tidal spectroscopy and prediction, *Philos. Trans. R. Soc. London, Ser. A, 259*, 533-581, 1966.

Oerlemans, J., Model experiments of the 100,000-yr glacial cycle, *Nature, 287*, 430-432, 1980.

Oerlemans, J., Glacial cycles and ice-sheet modelling, *Clim. Change, 4,* 353-374, 1982.

Oerlemans, J., The role of ice sheets in the Pleistocene climate, *Nor. Geol. Tidsskr., 71,* 155-161, 1991.

Oppo, D. W., R. G. Fairbanks, A. L. Gordon, and N. J. Shackleton, Late Pleistocene southern ocean $\delta^{13}C$ variability, *Paleoceanography, 5,* 43-54, 1990.

Peixoto, J. P., and A. H. Oort, Physics of climate, *Rev. Mod. Phys., 56,* 365-429, 1984.

Pestiaux, P., I. Van der Mersch, A. Berger, and J.-C. Duplessy, Paleoclimatic variability at frequencies ranging from 1 cycle per 10000 years to 1 cycle per 1000 years: Evidence for nonlinear behaviour of the climate system, *Clim. Change, 12,* 9-37, 1988.

Peterson, L. C., and N. B. Cofer-Shabica, Brunhes chron records of sedimentation and abyssal paleocirculation in the Venezuela Basin, eastern Caribbean Sea, *Geol. Soc. Am. Abstr. Programs, 19,* 804, 1987.

Pisias, N. G., and M. Leinen, Milankovitch forcing of the oceanic system: Evidence from the northwest Pacific, in *Milankovitch and Climate, Part 1,* edited by A. L. Berger et al., pp. 307-330, D. Reidel, Norwell, Mass., 1984.

Pisias, N. G., and D. K. Rea, Late Pleistocene paleoclimatology of the central equatorial Pacific: Sea surface response to the southeast trade winds, *Paleoceanography, 3,* 21-37, 1988.

Pisias, N. G., and N. J. Shackleton, Modeling the global climate response to orbital forcing and atmospheric carbon dioxide changes, *Nature, 310,* 757-759, 1984.

Pollard, D., A coupled climate-ice sheet model applied to the Quaternary ice ages, *J. Clim., 1,* 965-997, 1983.

Prell, W. L., and J. E. Kutzbach, Monsoon variability over the past 150,000 years, *J. Geophys. Res., 92,* 8411-8425, 1987.

Rasmusson, E. M., and T. H. Carpenter, Variations in tropical sea surface temperature and surface wind fields associated with the Southern Oscillation/El Niño, *Mon. Weather Rev., 110,* 354-384, 1982.

Raymo, M. E., Global climate change: A three million year perspective, in *Start of a Glacial,* vol. 3, edited by G. Kukla and E. Went, pp. 207-223, Springer-Verlag, New York, 1992.

Raymo, M. E., and W. F. Ruddiman, Tectonic forcing of late Cenozoic climate, *Nature, 359,* 117-122, 1992.

Raymo, M. E., W. F. Ruddiman, and P. N. Froelich, Influence of late Cenozoic mountain building on ocean geochemical cycles, *Geology, 16,* 649-653, 1988.

Raymo, M. E., W. F. Ruddiman, N. J. Shackleton, and D. W. Oppo, Evolution of Atlantic-Pacific $\delta^{13}C$ gradients over the last 2.5 m.y., *Earth Planet. Sci. Lett., 97,* 353-368, 1990.

Reid, J. L., and R. J. Lynn, On the influence of the Norwegian-Greenland and Weddell seas upon the bottom waters of the Indian and Pacific oceans, *Deep Sea Res., 18,* 1063-1088, 1971.

Ruddiman, W. F., and J. E. Kutzbach, Forcing of late Cenozoic northern hemisphere climate by plateau uplift in southern Asia and the American West, *J. Geophys. Res., 94,* 18,409-18,427, 1989.

Ruddiman, W. F., and A. McIntyre, Ice-age thermal response and climatic role of the surface Atlantic Ocean, 40°N to 63°N, *Geol. Soc. Am. Bull., 95,* 381-396, 1984.

Ruddiman, W. F., A. McIntyre, and M. Raymo, Paleoenvironmental results from North Atlantic sites 607 and 609, *Initial Rep. Deep Sea Drill. Proj., 94,* 855-877, 1986*a*.

Ruddiman, W. F., M. Raymo, and A. McIntyre, Matuyama 41,000-year cycles: North Atlantic Ocean and northern hemisphere ice sheets, *Earth Planet. Sci. Lett., 80,* 117-129, 1986*b*.

Ruddiman, W. F., M. E. Raymo, D. G. Martinson, B. M. Clement, and J. Backman, Pleistocene evolution: Northern hemisphere ice sheets and North Atlantic Ocean, *Paleoceanography, 4,* 353-412, 1989.

Saltzman, B., A survey of statistical-dynamical models of the terrestrial climate, *Adv. Geophys., 20,* 183-304, 1978.

Saltzman, B., and K. A. Maasch, Carbon cycle instability as a cause of the late Pleistocene ice age oscillation: Modeling the asymmetric response, *Global Biogeochem. Cycles, 2,* 177-185, 1988.

Saltzman, B., and K. A. Maasch, A first-order global model of late Cenozoic climatic change, *Trans. R. Soc. Edinburgh Earth Sci., 81,* 315-325, 1990.

Saltzman, B., and A. Sutera, The mid-Quaternary climatic transition as the free response of a three-variable dynamical model, *J. Atmos. Sci., 44,* 236-241, 1987.

Saltzman, B., and M. Y. Verbitsky, Multiple instabilities and modes of glacial rhythmicity in the Plio-Pleistocene: A general theory of late Cenozoic climatic change, *Clim. Dyn., 8,* 147-161, 1993.

Saltzman, B., A. Sutera, and A. R. Hansen, A possible marine mechanism for internally generated long-period climate cycles, *J. Atmos. Sci., 39,* 2634-2637, 1982.

Saltzman, B., A. Sutera, and A. R. Hansen, Earth-orbital eccentricity variations and climatic change, in *Milankovitch and Climate, Part 2,* edited by A. Berger et al., pp. 615-636, D. Reidel, Norwell, Mass., 1984.

Sarnthein, M., and R. Tiedemann, Younger Dryas-style cooling events at glacial Terminations I-VI at ODP site 658: Associated benthic $\delta^{13}C$ anomalies constrain meltwater hypothesis, *Paleoceanography, 5,* 1,041-1,055, 1990.

Savin, S. M., R. G. Douglas, and F. G. Stehli, Tertiary marine paleotemperatures, *Geol. Soc. Amer. Bull., 86,* 1499-1510, 1975.

Shackleton, N. J., Oxygen isotopes, ice volume and sea level, *Quat. Sci. Rev., 6,* 183-190, 1987.

Shackleton, N. J., and N. D. Opdyke, Oxygen isotope and paleomagnetic stratigraphy of equatorial Pacific core V28-238: Oxygen isotope temperatures and ice volumes on a 10^5 year and 10^6 year scale, *Quat. Res., 3,* 39-55, 1973.

Shackleton, N. J., and J. Imbrie, The $\delta^{18}O$ spectrum of oceanic deep water over a five-decade band, *Clim. Dyn., 16,* 217-230, 1990.

Shackleton, N. J., and N. G. Pisias, Atmospheric carbon dioxide, orbital forcing, and climate, in *The Carbon Cycle and Atmospheric CO_2: Natural Variations Archean to Present, Geophys. Monogr. Ser.,* vol. 32, edited by E. Sundquist and W. S. Broecker, pp. 303-317, AGU, Washington, D. C., 1985.

Shackleton, N. J., A. Berger, and W. R. Peltier, An alternative astronomical calibration of the lower Pleistocene

timescale based on ODP site 677, *Trans. R. Soc. Edinburgh Earth Sci., 81,* 251-261, 1990.

Shackleton, N. J., S. Crowhurst, T. Hagelberg, and N. G. Pisias, A new late Neogene time scale: Application to leg 138 sites, in *Proc. Ocean Drill. Program, Sci. Results,* edited by N. Pisias et al., College Station, Texas, 1993.

Short, D. A., J. G. Mengel, T. J. Crowley, W. T. Hyde, and G. R. North, Filtering of Milankovitch cycles by Earth's geography, *Quat. Res., 35,* 157-173, 1991.

Solheim, A., L. Russwurm, A. Elverhoi, and M. N. Berg, Glacial geomorphic features in the northern Barents Sea: Direct evidence for grounded ice and implications for the pattern of deglaciation and late glacial sedimentation, in *Glacimarine Environments: Processes and Sediments,* edited by J. A. Dowdeswell and J. D. Scourse, pp. 253-268, Geol. Soc. Spec. Publ. 53, London, 1990.

Sowers, T., M. Bender, D. Raynaud, Y. S. Korotkevich, and J. Orchardo, The $\delta^{18}O$ of atmospheric O_2 from air inclusions in the Vostok ice core: Timing of $CO_2$and ice volume changes during the penultimate deglaciation, *Paleoceanography, 6,* 679-696, 1991.

Stuiver, M., T. F. Braziunas, B. Becker, and B. Kromer, Climatic, solar, oceanic, and geomagnetic influences on Late-Glacial and Holocene atmospheric $^{14}C/^{12}C$ change, *Quat. Res., 35,* 1-24, 1991.

Tauxe, L., A. D. Deino, A. K. Behrensmeyer, and R. Potts, Pinning down the Brunhes/Matuyama and upper Jaramillo boundaries: A reconciliation of orbital and isotopic time scales, *Earth Planet. Sci. Lett., 109,* 561-572, 1992.

Taylor, C. A., *The Physics of Musical Sounds,* 196 pp., English University Press, London, 1965.

Turon, J.-L., Direct land/sea correlations in the last interglacial complex, *Nature, 309,* 673-676, 1984.

Weertman, J., Rate of growth or shrinkage of nonequilibrium ice sheets, *J. Glaciol., 5,* 145-158, 1964.

Weertman, J., Stability of the junction of an ice sheet and ice shelf, *J. Glaciol., 13,* 3-11, 1974.

Winograd, I. J., T. B. Coplen, J. M. Landwehr, A. C. Riggs, K. R. Ludwig, B. J. Szabo, P. T. Kolesar, and K. M. Revesz, Continuous 500,000-year climate record from vein calcite in Devils Hole, Nevada, *Science, 258,* 255-260, 1992.

Wright, D. G., T. F. Stocker, and L. A. Mysak, A note on Quaternary climate modelling using Boolean delay equations, *Clim. Dyn., 4,* 263-267, 1990.

Wunsch, C., and A. E. Gill, Observations of equatorially trapped waves in Pacific sea level variations, *Deep Sea Res., 23,* 371-390, 1976.

A. Berger, Institut d'Astronomie et de Géophysique G. Lemaître, Université Catholique de Louvain, 2, Chemin du Cyclotron, 1348, Louvain-la-Neuve, Belgium.

E. A. Boyle and M. E. Raymo, Department of Earth, Atmospheric, and Planetary Sciences, Massachusetts Institute of Technology, Cambridge, MA 02139.

S. C. Clemens, A. Duffy, J. Imbrie, and W. L. Prell, Department of Geological Sciences, Brown University, Providence, RI 02912.

W. R. Howard, G. Kukla, D. G. Martinson, A. McIntyre, B. Molfino, and J. Morley, Lamont-Doherty Geological Observatory of Columbia University, Palisades, NY 10964.

J. Kutzbach, Center for Climatic Research and Space Science, University of Wisconsin, Madison, WI 53706.

A. C. Mix and N. G. Pisias, College of Oceanography, Oregon State University, Corvallis, OR 97331.

L. C. Peterson, Rosenstiel School of Marine and Atmospheric Science, University of Miami, Miami, FL 33149.

N. J. Shackleton, Godwin Laboratory for Quaternary Research, Free School Lane, Cambridge CB2 3RS, United Kingdom.

J. R. Toggweiler, Geophysical Fluid Dynamics Laboratory, NOAA, Princeton, NJ 08542.

(Received April 30, 1993;
revised September 29, 1993;
accepted September 29, 1993.)